SEMMELWEIS EGYETEM

DOKTORI ISKOLA

Ph.D. értekezések

2990.

BARABÁS JÁNOS IMRE

Szív- és érrendszeri betegségek élettana és klinikuma
című program

Programvezető: Dr. Merkely Béla, egyetemi tanár

Témavezető: Dr. Hartyánszky István László, habil. egyetemi docens

OPTIMIZING THE PLACEMENT OF LEFT VENTRICULAR ASSIST DEVICES: A NOVEL APPROACH WITH PATENTED 3D TECHNOLOGY-ENHANCED SURGICAL TOOL

PhD thesis

Imre János Barabás

Doctoral School of Basic and Translational Medicine

Semmelweis University

Supervisor:	István Hartyánszky, MD, Ph.D
Official reviewers:	Tivadar Hüttl, MD, Ph.D
	Kálmán Benke, MD, Ph.D

Head of the Complex Examination Committee:
        Tivadar Tulassay, MD, D.Sc

Members of the Complex Examination Committee:
        Péter Andréka, MD, Ph.D
        Attila Patócs, MD, D.Sc.

Budapest
2023

Table of Contents

List of Abbreviations

2D	Two Dimensional
3D	Three Dimensional
3DPE	Three Dimensional Printed Exoskeleton
ACEI	Angiotensin-Converting Enzyme Inhibitor
ARB	Angiotensin-Receptor Blocker
BiVAD	Biventricular Assist Device
CAD	Coronary Artery Disease
CAVE	Computer-Assisted Ventricular Engineering
CFD	Computational Dynamic Simulation
CRT	Cardiac Resynchronization Therapy
CT	Computer Tomography
CTA	Computed Tomography Angiography
DICOM	Digital Imaging and Communications in Medicine
DSC	Dice similarity coefficient
EACTS	European Association for Cardio-Thoracic Surgery
EUROMACS	European Registry for Patients with Mechanical Circulatory Support
FDM	Fused Deposition Modelling
HD	Hausdorff-distance
HF	Heart Failure
IC	Inflow Cannula
ICD	Implantable Cardioverter Defibrillator
IVS	Interventricular Septum
LV	Left Ventricle
LVAD	Left Ventricular Assist Device
MRI	Magnetic Resonance Imaging
PhD	Doctor of Philosophy
PSM	Propensity Score Matching
RVAD	Right Ventricular Assist Device
SLA	Stereolithography
SLS	Selective Laser Sintering

STL	Standard Tessellation Language
VAD	Ventricular Assist Device
VE	Virtual Exoskeleton

1. INTRODUCTION

Heart failure has emerged as a globally significant and escalating cause of illness and death (1). Despite the ongoing advancements in both pharmaceutical and nonpharmaceutical treatments for heart failure, there is a rising number of patients being diagnosed with end-stage heart failure each year. Unfortunately, the preferred treatment option, heart transplantation, is impeded by the limited availability of donor hearts (2). To address this growing issue, an increasing number of patients are turning to mechanical circulatory therapy, which involves the implantation of left ventricular assist. These devices serve as life-saving interventions, offering temporary support until a successful heart transplantation can be performed or even as a long-term treatment strategy (3, 4). Furthermore, continuous developments in these devices are providing patients with a broader opportunity to return to an active everyday life (5).

The rotor of the mechanical heart is operated by a form of magnetic levitation technology. A transmission of kinetic energy to the blood flowing through the heart is provided by the rotor, to maintain the circulation of the patient. The inflow cannula is implanted into the apical part of the left ventricle. In this way, the blood is directed from the left ventricle into the rotor, through the inflow cannula, which is discharged through the outflow cannula, also known as the outflow graft. The outflow cannula is sewn to the ascending aorta (6). The left ventricle is effectively bridged by this solution, while the flow of venous blood, arriving from the lungs, is directed to the systemic circulation. The blood pressure of the patient is maintained by the left ventricular assist device with a continuous flow of blood, so it is not divided into a systolic and a diastolic phase.

An ideal functioning of the left ventricular assist device is achieved, if the axis of the inflow cannula is positioned approximately parallelly to the interventricular septum and facing the mitral anulus within the ventricle (7). It is elaborated by several international publications, that an inadequate functioning and serious complications can be caused by any deviation from the ideal positioning of the left ventricular assist device (8-10). One of the most serious consequences, and a life-threatening condition is caused by the pump when the vacuum in the pump pulls the lateral wall of the left ventricle or the interventricular septum towards to the inflow cannula, resulting in the immediate stoppage of the device. This phenomenon is known in international literature as the

"suction event". This complication can be presented by even 2-6% of the implantations, considerably increasing the risk of the operation (11). Moreover, further, long-term complications can be caused by any inadequate positioning. According to the 2020 study of Chivukula et al. (9), hydrodynamic parameters are significantly worsened by the inadequate position of the inflow cannula within the ventricle, significantly increasing the risk of thromboembolic complications. Increasing the long-term risk of microembolization, which could cause stroke in serious cases. The life expectancy of patients living with durable left ventricular assist device is reduced due to the inflow cannula malangulation and its complications (12).

Successful therapy with a left ventricular assist device is influenced by numerous factors, which can only be controlled with considerable difficulty (13). The geometric properties of the heart in question are to be underlined of these factors, which are heavily influenced by the existing pathological condition. A condition can be presented by restrictive or dilatative cardiomyopathy, characterized by pathological deviations in the tissue structure and the size of the heart (14). As a result, the capacity and internal structure of the left ventricle can be seriously altered in comparison to a normal, healthy heart.

Despite the continuous development of left ventricular assist device therapy, the unsolved nature of these problems is indicated by literary reviews on the subject. Currently, the implantation of the inflow cannula is supported by not quantifiable, intraoperative surgical experience to a considerable degree (15). However, an opportunity to preoperatively plan implantations, and to produce intraoperative surgical tools is provided by the processing of the image files of computer tomography examinations with 3D technology.

1.1. Heart Failure

1.1.1. Definition and Demographical Data

A worldwide significant and growing cause of morbidity and mortality is presented in the form of heart failure (HF) (1). Despite the continuously improving pharmacological and non-pharmacological therapies of heart failure, more and more patients are diagnosed with advanced heart failure every year, while the gold standard of treatment, heart transplantation is hindered by the limited number of available donor hearts (2). An increasing number of patients are treated with mechanical circulatory therapy, such as the left ventricular assist devices (LVADs), either as a life-saving intervention as temporal support until a successful heart transplantation, or as a long-term treatment strategy (4). Heart failure can be defined as a multifactorial medical syndrome, in which the blood-pumping function of the heart is compromised, leading to progressively worsening systemic perfusion and oxygenation. Diminishing contractile function, the remodelling of ventricular structures and neurohormonal deviations are all involved in the development of the syndrome (16). A serious global health challenge is presented by the prevalence and incidence of heart failure. The heart failure prevalence has undergone a substantial increase due to the reduced mortality rates of cardiovascular syndromes and the growth in the number of adults over 65 years in the population. In this age group, a notably elevated incidence of heart failure can be observed, which can be attributed to the presence of various comorbidities, and to the cardiovascular consequences of the human aging process (17).

The global heart failure epidemiological data were updated by Savarese and his colleagues in 2023 (18). It was revealed by the study that the prevalence of heart failure was found to be as high as 1-3% in the general adult population, with an increasing trend in its overall prevalence. Its incidence, however, was found to be stable, or even declining, with an incidence of 1-20 cases per 1000 person-years/per 1000 population. A serious problem is posed by the high mortality of heart failure: 30-day mortality was found to be around 2-3%, while 5-year mortality was found to be around 50-75%. An amount of 25.500 euros was calculated as the annual healthcare cost of heart failure, of which direct costs were found to be the main cost drivers, with around 70% of the whole costs. An already increasing trend can be noticed in the healthcare costs, caused by the major

demographic changes in developed societies, with other words, the increasing proportion of citizens older than 65 years.

The incidence and prevalence of the syndrome in Hungary are stated relying on the data of the first epidemiological study of heart failure in Hungary, which was conducted by Tomcsányi and Tóth in 2009 (19), and itself was based on the data of the National Health Insurance Fund Administration, and on the relevant data of the 2008 Hungarian Census. The epidemiological study of Tomcsányi and Tóth was followed by similar programs in Hungary in the last decade. One of these is the heart failure register, summarizing the data of ten medical centre's, which is regularly updated by the Gottsegen National Cardiovascular Centre. These projects are conducted independently from the data of the National Health Insurance Fund Administration. Therefore, a comprehensive picture of the epidemiology of heart failure is not presented by these surveys (20).

Over 155.000 citizens of Hungary were suffering from heart failure in 2009, according to the study of Tomcsányi and Tóth (19). The prevalence of heart failure was calculated by the authors, and a strong correlation between age and the prevalence of the syndrome was observed by them. The average prevalence of heart failure in Hungary was almost 1.58% according to the 2009 study. However, an overall prevalence of HF 5.5% was observed in the population involved in the Budakalász Epidemiology Study (21). The incidence of heart failure in Hungary was first calculated by Tomcsányi, and an incidence of 33.960, that is, 0.34% of the Hungarian population was stated by him. However, Tomcsányi and Tóth indicated that the actual prevalence data should be estimated as substantially higher than that. The reasons behind this phenomenon were given as the dominance of hospital discharge records as sources of the data, which can be distorted by various inaccuracies, the sporadic nature of patient care and the fact that the study was a short-term one.

1.1.2. Therapeutic Options

Prevention is increasingly seen as crucial in the management of the syndrome. The prevention of overweight and obesity, a physically active lifestyle, sufficient rest, smoking cessation and the control of blood pressure are all regarded as beneficial lifestyle changes, by which the individual risk of heart failure can be seriously decreased (22).

The first-line treatment is represented by pharmacotherapy (23). Medications with an ability to modulate neurohormones involved in the development of heart failure are regarded as the essential tools of basic heart failure-treatment. All such medications are characterized by a mechanism of effect of blocking or inhibiting the neurohormones. Aldosterone antagonists, angiotensin-receptor blockers (ARBs), angiotensin-converting enzyme inhibitors (ACEIs), and β blockers are all included in this group (24-27).

Complementary therapy options are non-pharmacological therapies (28). Implantable cardioverter defibrillators (ICDs) are increasingly used in the prevention of sudden cardiac death, as their efficacy in this role was demonstrated by multiple randomized controlled studies (29, 30).

A substantial subgroup of patients (20-30%) with heart failure are suffering from an intraventricular conduction delay (31). This condition may compromise the circulatory function of the heart even further and can lead to a regurgitation through the mitral valve, exacerbating the symptoms of heart failure. It can be treated with cardiac resynchronization therapy (CRT), which is based on the simultaneous pacing of the left and right ventricles (or of a sole ventricle, if a bundle branch block is present), reducing dyssynchrony.

Advanced heart failure in many cases is characterized by a refractory nature, despite optimized pharmacotherapy, and non-pharmacological therapies. In these cases, different forms of mechanical circulatory support can be used. Here we distinguish between short-, medium- and long-term devices. Short-term devices include ECMO, while medium-term devices include various assist devices. These are not fully implantable devices, but they help to stabilise patients until transplantation. Long-term devices include the durable left ventricular assist device, which are fully implantable and can support the patient's circulation for months or years. These devices make it possible for patients who originally may not have been suitable for transplantation to undergo a heart transplant after the device implantation. The detailed description these devices will be presented in Chapter 1.2.

Such cases can be managed either by mechanical circulatory support, or by cardiac transplantation. In the last decade, the number of available donor hearts was found to be decreasing (32). Over the past decade, LVAD implants have seen a significant rise, as indicated by the European Registry for Patients with Mechanical Circulatory Support

(EUROMACS) reports published by the European Association for Cardio-Thoracic Surgery (EACTS) (33, 34). While the overall implantation numbers remain consistent by years, there's a notable and steady increase in the annual implantation of continuous flow–full magnetic levitation devices like the HeartMate 3 among European centres who provided data to the registry from 2013 (34).

Left ventricular devices come in various forms, each designed for specific durations of support, including short-term, midterm, and long-term assist devices. These devices differ based on their intended duration of use (3). Most of such devices are implanted into the left ventricle, as more than 50% of patients suffering from advanced-stage heart failure are diagnosed with failing left heart syndrome and are called left ventricular circulatory device for this reason.

1.2. Types of Mechanical Circulatory Support devices

Extracorporeal Membrane Oxygenation (ECMO) plays a pivotal role in managing heart failure cases unresponsive to conventional treatments. It serves as a temporary life support system by diverting deoxygenated blood from the right atrium or vena cava, oxygenating it, and returning it to the arterial system (veno-arterial or central ECMO, supports both heart and lung function). The other type of ECMO therapy is the veno-venous ECMO, supports lung function primarily (35). In this setup, the support is achieved with two venous cannulas, one usually inserted in the right femoral vein and the other inserted in the right internal jugular vein and advanced through the superior vena cava into the right atrium. Patient selection is paramount, with ECMO considered for those with severe, refractory heart failure, ineligible for immediate transplantation, or having potentially reversible causes. The ECMO circuit consists of venous and arterial cannulation, a membrane oxygenator, a pump, and monitoring systems, ensuring proper gas exchange and patient stability. However, ECMO is not without complications, including bleeding, infection, and embolic events. Nevertheless, it offers a lifeline, improving outcomes by providing a bridge to recovery, transplantation, or ventricular assist devices, underscoring its critical role in the heart failure management landscape (36).

The ventricular assist devices (VAD) are mechanical pumps employed in the augmentation of cardiac function and circulatory support for patients with cardiac insufficiency (37). This apparatus extracts blood from the cardiac ventricle and propels it throughout the body, facilitating circulation to vital organs, emulating the hemodynamic performance of a normally functioning heart.

Ventricular assist devices can be categorised according to several aspects. They are commonly used in medium-term duration (between weeks and months), and the pumps are not implantable. They can be categorised by the supported ventricle: left ventricle assist device (LVAD), right ventricle assist device (RVAD) and biventricular assist device (BiVAD). A short list of these pumps can be seen on *Table 1*. The **long-term ventricular assist devices** are utilized in cases of advanced heart failure when conventional therapies have proven ineffective (38). It is employed as a bridge to transplantation for patients awaiting a heart transplant or as destination therapy for those who are ineligible for transplantation. The LVAD is surgically implanted and assists the heart's pumping function, significantly improving the patient's quality of life and overall survival. It functions by drawing blood from the left ventricle and propelling it into the aorta, thus enhancing systemic circulation. Long-term LVAD therapy has become a valuable option, offering extended support and hope for patients with end-stage heart failure. In the realm of the ventricular assist devices, two fundamental types exist: the left ventricular assist device and the right ventricular assist device. Combining both is termed a biventricular assist device; however, it does not represent a distinct VAD category. The LVAD is the predominant type, augmenting left ventricular function to propel blood into the aorta, the primary conduit for oxygen-rich blood distribution throughout the body. RVADs are typically employed for short-term right ventricular support post-LVAD or other cardiac surgeries, assisting in blood flow to the pulmonary artery for oxygenation. When both ventricles exhibit insufficient function, both LVAD and RVAD, or a BIVAD, may be implemented, with a total artificial heart presenting an alternative treatment for such cases.

The durable left ventricle devices can be used as long-term mechanical circulatory support. Detailed description can be found in *Chapter 1.2.1*.

Table 1. The list of the short-, and long-term ventricular assist devices. * Devices are no more accessible for clinical purposes (39).

Types of Devices Based on Duration				
Short-term Devices	Long-term Devices			
	Pulsatile Flow	*Axial continous flow*	*3rd generation LVADs*	*Total Artificial*
TandemHeart				
Abiomed Impella	Thoratec HeartMate XVE	Thoratec HeartMate II*	HeartWare HVAD*	Syncardia
Heartmate PHP	Thoratec paracorporeal VAD	Jarvik 2000	DuraHeart	
Abiomed BVS500	Thoratec inracorporeal VAD	MicroMed Dabakey	Thoratec HeartMate III	
Abiomed AB50000 CentriMag				

Therapeutic indications are the other type of categorisation. There are also called as bridge strategies (3):

The "**Bridge to Bridge**" strategy involves a transition to a long-term left ventricular assist device following a period of stabilization with temporary surgical mechanical circulatory support lasting several months (40).

In a "**Bridge to Decision**" scenario, a pivotal clinical decision regarding the next steps, specifically the selection of definitive therapy, is imminent. However, before proceeding with the definitive treatment, the patient necessitates temporary mechanical circulatory support to maintain their hemodynamic stability during the decision-making process (41).

The "**Bridge to Recovery**" strategy is designed to facilitate a patient's expected recuperation. Before a full recovery can occur, essential support is provided to guide them through a life-threatening period. An example of this strategy could be the utilization of ECMO in cases of fulminant myocarditis (42).

The "**Bridge to Candidacy**" strategy pertains to a situation where the health status of the patients precludes them from being a suitable candidate for heart transplantation. However, this strategy aims to transition the patient to a state where they become eligible for the intended therapy. For example, the use of ECMO to facilitate a patient's readiness for nontransplant cardiac surgery (43).

The "**Bridge to Transplant**" strategy aims to maintain a patient's health at an adequate level for an extended duration, allowing them to remain eligible for organ transplantation while awaiting the availability of a suitable organ (44).

1.2.1. Description of the durable LVAD system

Table 1. shows the long-term (also called durable) VADs. Although the main difference is the flow pattern provided by the pump, the mechanical mechanism inside the devices is the same technology: the magnetic levitation rotor. This rotor uses a permanent magnet to create a constant magnetic flux that spreads radially from the inside of the rotor, allowing the rotor to be controllably levitated by bipolar direct current magnetic fields (45). This reduces the shear stress on the blood cells, thereby reducing thrombus formation. As a result, the incidence of stroke, pump thrombosis and mucosal bleeding is reduced (46).

The basic structure of a left ventricular assist device can be divided into the mechanical pump, the inflow cannula, the outflow graft and the driveline. These main parts are shown by *Figure 1.* in virtual three dimensional (3D) model.
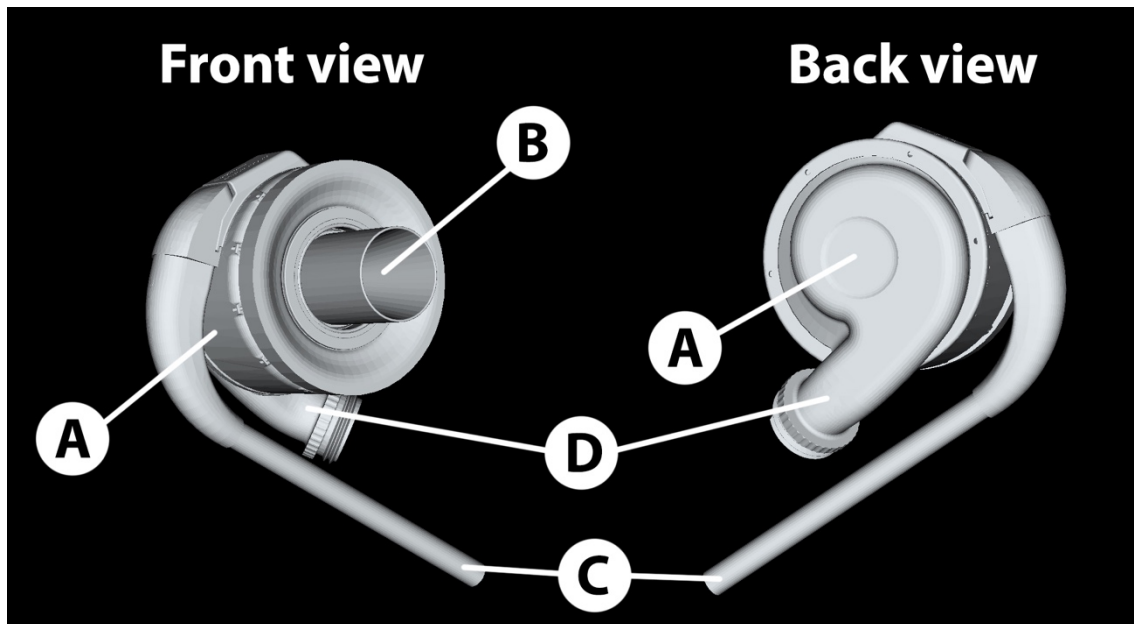

Figure 1. Virtual 3D model of the left ventricle assist device. A: Pump, B: Inflow cannula, C: Driveline, D: Outflow cannula (47).

The circulation of the patient is supported by the kinetic energy generated by the mechanical pump The mechanical pump, basically a rotor, is powered by a form of magnetic levitation technology. The inflow cannula is inserted through the apex of the left ventricle. As a result, blood is led out from the left ventricle, through the inflow cannula and the rotor, reaching the bloodstream via the outflow graft. The list of the main parts of the left ventricular assist device is closed by the driveline, which connects the pump with the outer energy source (48).

Despite advancements in hemocompatibility, right heart failure and infections, the followings are remained as an unresolved problem such as the simultaneous two-chamber support, wireless so-called transcutan charging and automated flow rate modulation according to the physical demand. These developments are currently underway and are likely to be available in the near future for everyday clinical practice (46, 49).

1.2.2. Importance of the Inflow Cannula Position

The thrombogenicity associated with ventricular assist devices remains a pressing concern, in conjunction with adverse events. Among these, stroke, regarded as one of the most severe complications (50), are likely attributed to thrombus deposition within the supported ventricle around the inflow cannula. This thrombotic risk is exacerbated by non-physiological intraventricular flow patterns (51, 52) in VAD patients, which lead to the formation of stagnant regions (8). Moreover, observations of thrombus growth on the outer surface of the inflow cannula (52) have raised multiple critical hypotheses. These include patient-related factors such as intrinsic hypercoagulability and hypertension, as well as management factors like the anticoagulation regimen. Furthermore, the orientation of the inflow cannula concerning the mitral valve (53), the ventricle size (53), the insertion depth of the inflow cannula, the structural properties of the cannula's outer surface, and the positioning of the cannula are all implicated as potential contributing factors (54).

The success of heart failure therapy with left ventricular assist device is heavily influenced by the adequate position of the inflow cannula, which should be positioned

pointing to the center of the mitral valve, parallelly to the interventricular septum. As it is corroborated by the relevant medical literature, the optimal entry position for the inflow cannula is achieved, if an angle between -7 degrees and +7 degrees is closed by it and the interventricular septum, counted from the left ventricular septal axis (53). With an entry position within these values, favourable postoperative fluid mechanics can be achieved inside the left ventricle, and potentially life-threatening complications can be avoided (12). One of the most dangerous complications following the implantation is the suction event, when the mechanical pump is immediately stopped, as the interventricular septum is drawn to the mouth of the inflow cannula (11).

1.3. Radiological Assessment in Advanced Heart Failure
1.3.1. Preoperative CT scans in LVAD Candidates

The diagnosis and all the decision makings in advanced heart failure patient management are heavily based on cardiac imaging (55). The first-line method of investigating abnormalities in ventricular function, if heart failure is suspected, is echocardiography, as it is stated by the current guidelines of the European Society of Cardiology (56, 57). In cases complicated by problematic echocardiographic windows, or if the myocardium is to be examined, or the presence of complex congenital heart disease is suspected, cardiac magnetic resonance imaging (MRI) is to be applied. In patients with a low to intermediate risk of obstructive coronary artery disease (CAD), cardiac computed tomographic angiography (CTA) is given an isolated Class IIb indication, for excluding the syndrome (57).

In the past ten years, multiple substantial achievements have been reached in the field of cardiac computed tomography. Temporal resolution was improved by single X-ray tube scanners (from <500 msec to 250 msec), scanning single heart beats (320 slices) was made possible by better detectors, improved spatial resolution enabling the scanning of structures down to 0.3mm was achieved, while dual source CT (temporal resolution down to 66 msec) was developed. 3D reconstruction algorithms have been increasingly used in the treatment of heart failure, enabled by improved computational processing abilities.

Nowadays, contrast enhanced CTA imaging is utilized as a standard diagnostic tool in most heart failure centres (58, 59).

1.3.2. Postoperative CT Assessment of the LVAD Device

With more and more patients being treated with durable LVAD devices, the comprehensive functionality of such devices has been made a subject of increased investigation. As a result of this attention, multiple potential short- and long-term complications have been identified, including life-threatening ones, such as infection, malposition of the cannula and thromboembolism. Previously adverse events were identified by echocardiography manly Today high-resolution imaging of cardiovascular structures in a noninvasive way became possible by electrocardiogram gating CTA (60). The CTA is neither limited by suboptimal acoustic windows, nor hindered by acoustic shadowing, thus better visualization of LVAD cannula can be achieved (61).

1.4. The 3D technology from Planning to 3D Printing

The application of 3D technology to medical problems is characterized by rapid development and a wide range of opportunities (61). Visualization in 3D in the virtual space, modelling and 3D printing are powerful tools to offer anatomical reconstruction of complex structures of the human body, ranging from pathologies through single organs to complex anatomical structures (62). Simulation in the virtual space can be used to recreate both normal and pathological processes in the patient, with very high accuracy. Models specific to individual patients can created, extending the frontiers of personalized treatment. Furthermore, anatomical models printed in 3D have a considerable educational potential, helping medical specialists in understanding anatomy or pathology (63). Discoveries in medicine can be accelerated and patient outcomes can be improved by medical 3D technology.

1.4.1. Medical 3D Modelling Process

The initial step in medical 3D modelling is obtaining high resolution medical imaging data. The utilized data sources in the field often encompass computed tomography scans, MRI scans, ultrasound, echocardiography or digital pictures. Every imaging modality offers distinct information regarding the anatomical features of the patient, enabling thorough evaluation.

After acquisition of medical images, the subsequent stage entails the process of data segmentation. During this stage specific software is utilized to demarcate the areas of interest within the photographs. The segmentation process involves the separation of anatomical structures from surrounding tissues and artifacts, resulting digital representation of the structures of interest (64).

After segmentation, the resulting data is utilized to construct a 3D representation of the anatomical structure. The process of reconstruction employs mathematical algorithms to transform the two-dimensional image slices into a unified 3D representation. The generated model exhibits a high-level accuracy in the dimensions, form, and spatial interconnections of the structure under investigation.

Subsequently, the 3D models undergo virtual exploration. This enables healthcare professionals to engage with and assess the anatomical structures from diverse viewpoints and vantage points. The utilization of 3D imaging techniques enables a more comprehensive understanding of anatomical interconnections and deviations that may not be obvious in two-dimensional (2D) representations.

1.4.2. Medical 3D Printing

In certain instances, there is a need to generate a palpable 3D model via 3D printing, as physical models offer a heightened degree of intricate information. The printing method must comply with the current medical device regulation guidelines (65). In the European Union, medical devices produced by 3D printing technology are subject to a conformity assessment process. This evaluation is conducted to verify that these devices adhere to the legal standards, thereby ensuring their safety and intended functionality. In Hungary,

the first stage of the process entails the clinical assessment of the device, after obtaining approval from the ethical committee at Semmelweis University. Our research was built upon a previous clinical inquiry that examined the clinical viability of utilizing 3D reconstruction in surgical procedures for left ventricular aneurysms (66).

The technique of 3D printing involves the utilization of a diverse range of materials, such as biocompatible polymers, metals, ceramics, and even biological substances (67-70). The deposition of these materials occurs in a sequential manner, with each layer being carefully directed by the digital model, resulting in the formation of the tangible thing. Various printing processes are utilized by 3D printers, including fused deposition modelling (FDM), stereolithography (SLA), and selective laser sintering (SLS), which are chosen based on the unique application and material needs (66). Following the printing process, the manufactured object frequently necessitates other procedural measures, including cleaning, surface refinement, and sterilization, to guarantee its compliance with the requisite medical standards and safety prerequisites.

1.5. Flow simulations of the Inflow Cannula

Chivukula et al. (9, 53, 71) were the first, who used computational fluid dynamical simulation in durable LVAD implantation to evaluate the inflow cannula position and its effect on intraventricular flow pattern and postoperative complications. Their work focused on three main aspects of the flow pattern in left ventricle, which was also important in our research work:

> 1. The **ventricular size** and its global geometry are independent risk factor for ventricular assist device thrombosis. In 2019, it was concluded that left ventricle hemodynamic profile differs markedly based on LV chamber size and geometry. In VAD patients with small LVs, the flow pattern facilitates platelet activation and aggregation, resulting in thrombus formation. This markedly increases the risk of device thrombosis and neurologic events for VAD patients with small LVs, or patients whose LVAD decreases due to reverse remodelling on support (71).

2. The inflow **cannula insertion depth** significantly increases the postoperative thrombosis risk. The blood flow patterns within the left ventricle are profoundly impacted by inflow cannula insertion depth. Nearly four times as many platelets were trapped around the inflow cannula if it was deeper in the ventricle cavity, compared with reduced depth scenario. The deeper depth leads to a higher risk of platelet activation, thrombosis, and stroke (9).

3. The **malangulation** of the inflow cannula proved to be the cause of the unfavourable left ventricle hemodynamic changes after the implantation (53). This malangulation strongly impacts platelet activation and increases risk of thrombosis. Chivukula et al. (53) study provided quantitative evidence linking the degree of inflow cannula angulation to risk of thrombosis: an angle of $0\pm7°$ from the LV apical axis toward the mitral annulus is most biocompatible and significantly reduces thrombogenic flow patterns. Outside this angle range, the possibility of postoperative complications significantly increases. This study concluded that the inflow cannula must face to the central point of the mitral annulus, thus minimizing the risk of device thrombosis and cerebrovascular accident.

The positioning of the durable LVAD inflow cannula directly influences the flow pattern within the left ventricle, impacting the effectiveness of treatment. An angle exceeding $14°$ between the inflow cannula and the interventricular septum may result in postoperative complications due to the potential formation of stagnant regions around the cannula inside the left ventricle, elevating the risk of thrombosis. Conversely, maintaining a parallel alignment or an angle of less than $7°$ between these elements can minimize turbulence and stagnation. Consequently, reducing the risk of postoperative adverse events.

Furthermore, the internal geometry and specific anatomical structures within the left ventricle, including papillary muscles, trabeculae, interventricular septum, and mitral annulus, significantly influence the optimal positioning of the inflow cannula (58, 71). Achieving favourable patient outcomes and reducing complications depend on precisely positioning the inflow cannula to ensure appropriate interventricular flow dynamics and enhanced postoperative results. A comprehensive understanding of how the angle of the inflow cannula impacts flow dynamics is crucial for determining the most effective therapeutic options for our patients.

In addition, the precise utilization of the experience gained with the correct positioning of the cannula during surgery has not been solved so far. Although the clinical and theoretical studies (as can be read in the previous chapters of the thesis) clearly determined the accurate position of the inflow cannula, this knowledge could not be applied during the durable LVAD implantation. We developed our solution for this unmet medical need.

2. OBJECTIVES

Our research aim was to develop a new method, in which the assisted implantation of the left ventricular assist device is made possible by preoperative planning with 3D technology, thus, the potential complications resulting from the malposition of the durable LVADs would be reduced.

Our work was built up around three main goals.

1. The **primary goal** was to build a 3D modelling and 3D printing method to pioneer individualized models at Semmelweis University based on the development of an anatomically precise 3D modelling computational method.

2. The **second goal** aimed to calculate the optimal durable LVAD position inside the left ventricle, utilizing the previously developed method to create patient-specific 3D models. A surgical instrument was also developed, facilitating the optimal position coordinates transfer to the surgical field. This instrument, referred to as the Exoskeleton, allows for precise intraoperative implantation of the durable LVAD based on the calculated coordinates. The technological framework will be presented making possible the production of the Exoskeletons for durable LVAD implantation and analysing the accuracy of the printing process through the comparison of the 3D printed Exoskeletons and their original 3D-models.

3. The **third goal** was the analysis of postoperative outcomes by an evaluation of outcomes in patent group operated on, using 3D printed Exoskeletons

3. **METHODS**

To enhance comprehension of our research methodology, the methods chapter is structured into three parts. The initial part delineates the description of general 3D modelling and its precision assessment. The second part details the methodology for positioning a durable LVAD in-silico, along with the introduction of a novel 3D printed surgical tool—the Exoskeleton design—and its quality evaluation. Finally, the third part presents the postoperative outcomes observed through clinical utilization of the Exoskeleton.

3.1. METHODS – PART I: Individualized 3D models

Our research focused on developing a precise method to generate 3D anatomical models from medical images. This method was subsequently adapted for various medical specialties including general surgery, orthopedic surgery, gynecology, pediatric surgery, and congenital cardiac surgery at Semmelweis University.

3.1.1. DICOM data for 3D modelling

Throughout the medical image gathering process, the data pertaining to the produced images undergoes multiple steps prior to the development and production of tailored 3D models. The preliminary stages of 3D modelling and printing entail acquiring appropriate CT angiographic scans. The resulting images are recorded in the Digital Imaging and Communications in Medicine (DICOM) format, which encapsulates the medical imaging data. From mathematical perspective, these file formats contain coordinate data that represents distinct grey shades. Specifically, Hounsfield units are used for CT pictures, intensity values for MRI images, and density values for ultrasound images. These data are organized inside a matrix framework. This matrix represents a composite of horizontal planes, illustrating the analyzed organ or organ systems in a sequential manner along the z-axis. The individual cells present in the matrices possess an excess of information that surpasses what can be perceived using normal medical picture visualization or typical 3D rendering tools (72).

By utilizing image processing technologies and doing finite element analysis of flow dynamics, it is possible to construct dynamic 3D models by additional mathematical manipulation of the data. These models have the potential to enhance functional evaluations, therefore opening new opportunities for patient treatment and research activities.

3.1.2. The 3D Segmentation Procedure

Segmentation involves the computational analysis of image data, assigning functional units to consecutive horizontal layers. This process selects only the specific areas relevant to the 3D design within each layer. Referred to as the region-of-interest (ROI), this area can encompass various structures. The delineation of this region can be achieved through three methods: manual, automatic, or semi-automatic techniques (*Figure 2.*):
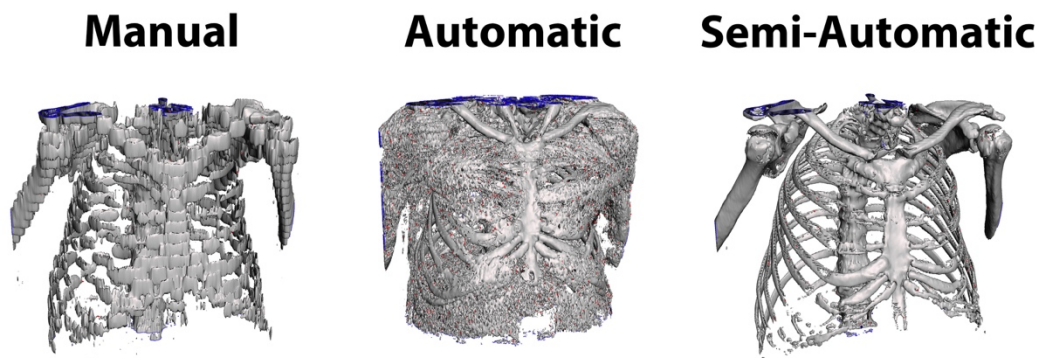

Figure 2. Visual representation of various segmentation techniques: A: Manual segmentation, B: Automatic segmentation, C: Semi-automatic segmentation technique.

In manual segmentation, we go through each layer individually and mark out the structure intended for 3D modelling. The drawback of this segmentation technique is its time-consuming nature, and the resulting 3D model surface tends to be stepped or jagged due to software limitations preventing the smoothing or correction of surface wrapping curves (*Figure 2/A*).

During automatic segmentation, the software identifies specific areas of the image according to the settings. The most common setting involves marking a certain range of gray shades (threshold) within the entire image (73). The threshold is based on Hounsfield

units in CTA images. The advantage of this technique is its speed, but the downside is that the resulting 3D model contains artifacts, requiring extensive post-processing. This occurs because the image not only contains the designated range of Hounsfield units within the intended modelling area but also includes unrelated points that manifest as artifact during modelling (*Figure 2/B*).

The third method is semi-autonomous segmentation. This approach combines the advantages of both manual and automatic segmentation techniques. It allows for the rapid creation of anatomically accurate and artifacts-free 3D models (*Figure 2/C*).

Within the semi-autonomous technique, our team utilizes MATLAB-based source code. Employing a modified form of the Kalman filter principle (74), this approach selects not only the specific Hounsfield unit range within the layers of DICOM files but also performs recursive estimation between individual points and their neighboring points. This method computes the relationship between the voxels not only on the same layer but in 3D shape (sphere-shape calculation). This specific structure (ROI) is created by applying the relevant mathematical formula:

$$F_k = \frac{\partial f(k)}{\partial x} \cdot x = x(k \cdot k),$$

$$H_{(k+1)} = \frac{\partial f(k+1)}{\partial x} \cdot x = x(k+1 \cdot k),$$

where to use of F_k as the state-transition matrix, defining the designated area, and $H_{(k+1)}$ as the observation matrix, which corrects the designated area at point $(k + 1)$. In complex anatomical structures or cases of tumor infiltration, utilizing the modified Kalman filter enables more precise differentiation of tissue boundaries, facilitating more accurate 3D reconstructions (73, 74). Subsequently, virtual 3D objects are created from the designated areas. During this process, a grid is defined along the surface curves of the designated volumetric layers, forming triangles of specific sizes (*Figure 3*).
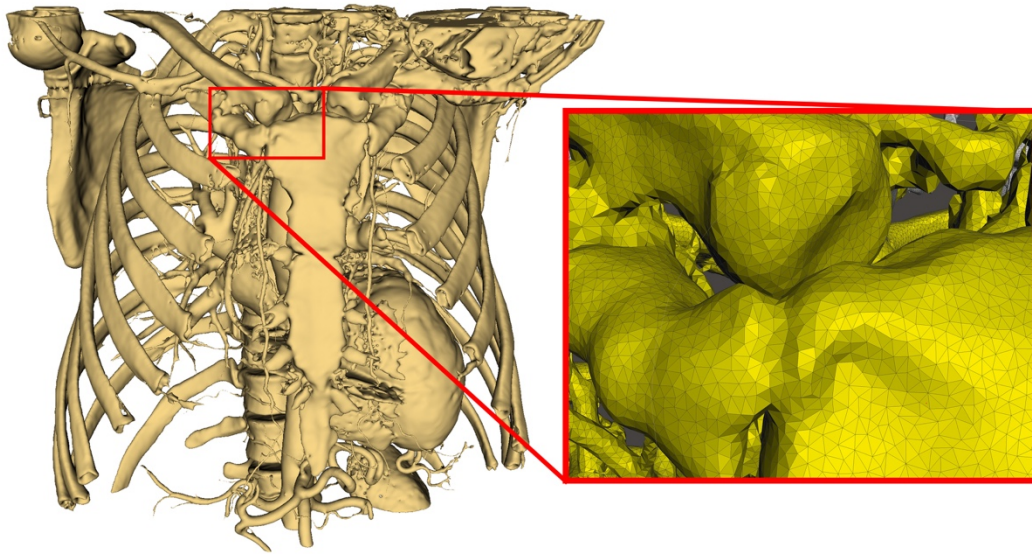
Figure 3. Triangle formation on the surface of the 3D model. The size and the accuracy of the 3D models depends on the size and consequently the number of the triangle. A precise model consists more and smaller triangles.

These triangles' coordinates are saved in Object format with texture, enabling the printing of models or projection onto devices suitable for displaying virtual reality (66). The Object format allows for the transformation into a 3D printable STL file without texture. At the following steps, we can accurately print the created 3D models to the intended size as planned using the patient's CTA data.

3.1.3. The 3D Printing Technologies

3D printing belongs to the group of prototyping processes, also known as additive manufacturing technologies. It's considered an indispensable tool in both industrial and medical technology, often regarded as a crucial aspect of the fourth industrial revolution. Unlike traditional manufacturing methods, which involve shaping an object from one or more pieces, 3D printing builds objects layer by layer. Its advantages over conventional industrial production methods include speed and lower material costs.

Its medical applicability arises from the micrometer-level printing precision and the substantial flexibility in creating various shapes. By selecting the appropriate printing type, it's possible to 3D print any human organ with anatomical accuracy, or even surgical

instrument and guiding tools. Three types of 3D printing technologies have gained prominence in medical applications. These types differ in their printing technology, resolution, printing speed, and the materials used (*Table 2*) (66).

	Fused Deposition Modeling (FDM)	Stereolithography (SLA)	Selective Laser Sintering (SLS)
Table 2. Shows the specifications of the most commonly utilized 3D printing technologies in the medical field.			
Printing volume	Small	Small	Big
Printing time	Long	Short	Very long
Surface finish	Very Robust	Thin	Thin
Raw material	Thermoplastic	Resin	Composit or Metal powder
Medical usage	Anatomical models Education Rapid prototyping	Surgical guides Detailed anatomical models	Implantation Prostetics
Printing price	Low	High	Very High

Fused Deposition Modelling (FDM) is a popular 3D printing technology that works by extruding melted thermoplastic filament through a heated nozzle onto a build platform. First, the 3D model is sliced into layers using specialized software. The FDM printer then heats the filament to its melting point, turning it into a semi-liquid state. The nozzle moves along the X, Y, and Z axes, depositing the melted filament layer by layer onto the build platform according to the sliced design. As each layer is deposited, it quickly cools and solidifies, fusing with the preceding layers. The heated build platform aids in adhesion and prevents warping by maintaining a controlled temperature. FDM printers use support structures, often made from the same material, to provide stability for overhanging sections of the design during printing. Once printing is complete, the object may undergo post-processing steps like removal of support structures, sanding, or surface finishing for a polished final product (75). FDM technology is primary used for anatomical model printing and as education models during graduate and postgraduate courses.

Stereolithography (SLA) is another type of 3D printing technology that applies photopolymerization, using a process involving light-sensitive liquid resin. The SLA printer begins by preparing a reservoir containing liquid photopolymer resin, typically placed in a tank. A precise UV laser is then used to selectively cure or solidify specific areas of the liquid resin. This light exposure occurs according to the cross-sectional layers of the 3D model, dictated by slicing software. As the laser scans or traces each layer's pattern onto the liquid resin surface, the cured layers gradually build upon one another,

forming the object. The building platform, often connected to a vertical elevator system, incrementally moves or lifts to allow for the formation of each new layer. Once the printing process is complete, the object is raised out of the tank. The printed object may undergo post-curing processes, such as isopropyl alcohol washing to remove the non-photopolymerized resin and additional UV light expose to fully harden and strengthen the resin (76). SLA printing enables high-resolution prints with intricate details, making it suitable for applications like surgical guides.

Selective Laser Sintering (SLS) is the most powerful 3D printing technology in medical usage. It is fusing powdered materials, typically polymers or metals, to create solid objects. The process initiates with a thin layer of powdered material spread across the build platform. A high-powered laser is then precisely guided by a computer-controlled system to selectively sinter or fuse the powdered material, binding it together to form the object's cross-section based on the digital printing data (STL). Once the first layer is sintered, the build platform descends, and a fresh layer of powder is distributed, repeating the process for each subsequent layer. Once printing is complete, the object is extracted from the powder bed and undergoes post-processing to remove excess powder. SLS allows for the creation of complex, intricate designs with high accuracy and strength due to the solidification of each layer within the powder bed (77). This technology is widely used in various industries, including aerospace, automotive, and medicine, for manufacturing functional prototypes, end-use parts, and components requiring robustness and intricacy. The versatility of SLS in working with a range of materials, including polymers and metals, makes it a valuable choice for producing diverse objects with different mechanical properties.

3.1.4. Tumor Segmentation and Volume Calculation

In cases involving tumors, DICOM data sourced from MRI images was preferred due to its superior tissue resolution compared to alternative medical imaging modalities. All of the tumor was a solid, well demarked tumor, where the tumor tissue was easily separable form the healthy tissue. It ensures the accuracy of the following volume comparison. The MRI resolution facilitated a clearer differentiation between the tumor and the neighboring tissue structures. The precision of the 3D models was evaluated by comparing the

intended and actual characteristics, encompassing the location, shape, and volume of the excised tumors. A total of 18 tumor cases were reconstructed in 3D, 11 of them were printed in 3D using FDM technology (*Figure 4.*).
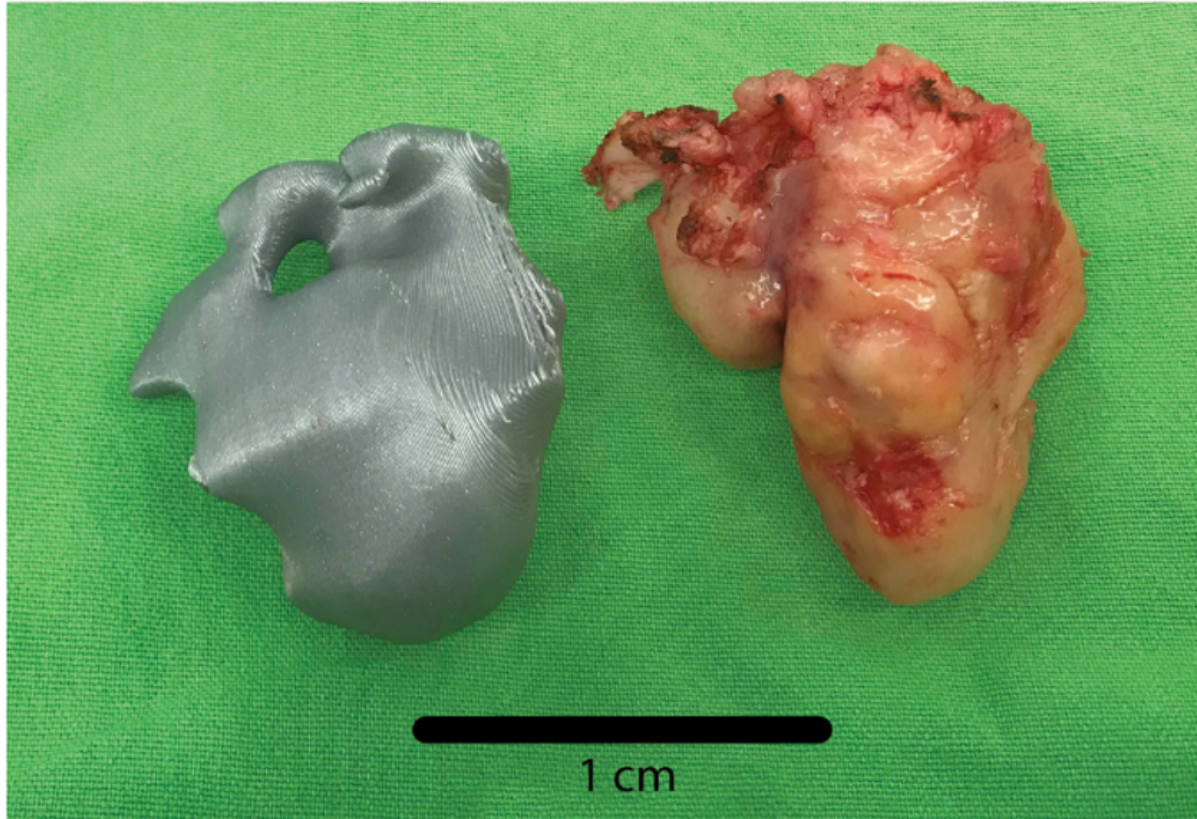

Figure 4. Comparison of the tumor model, represented by the grey object on the left side of the image, with the excised tumor tissue depicted on the right side (66).

The tumor volume was measured during the pathology examination, using the water displacement phenomenon. Submerged the removed tumor in a container of water, capturing the water displaced by the tumor mass. The volume of water displaced was equal to the volume of the object.

In silico, the tumor volume was calculated as sum of the voxels, because the tumor was represented in a grid of voxels in the 3D model. The volume is determined by counting the number of voxels within the object and multiplying it by the voxel volume. The voxel calculation method is presented in *Figure 5*.
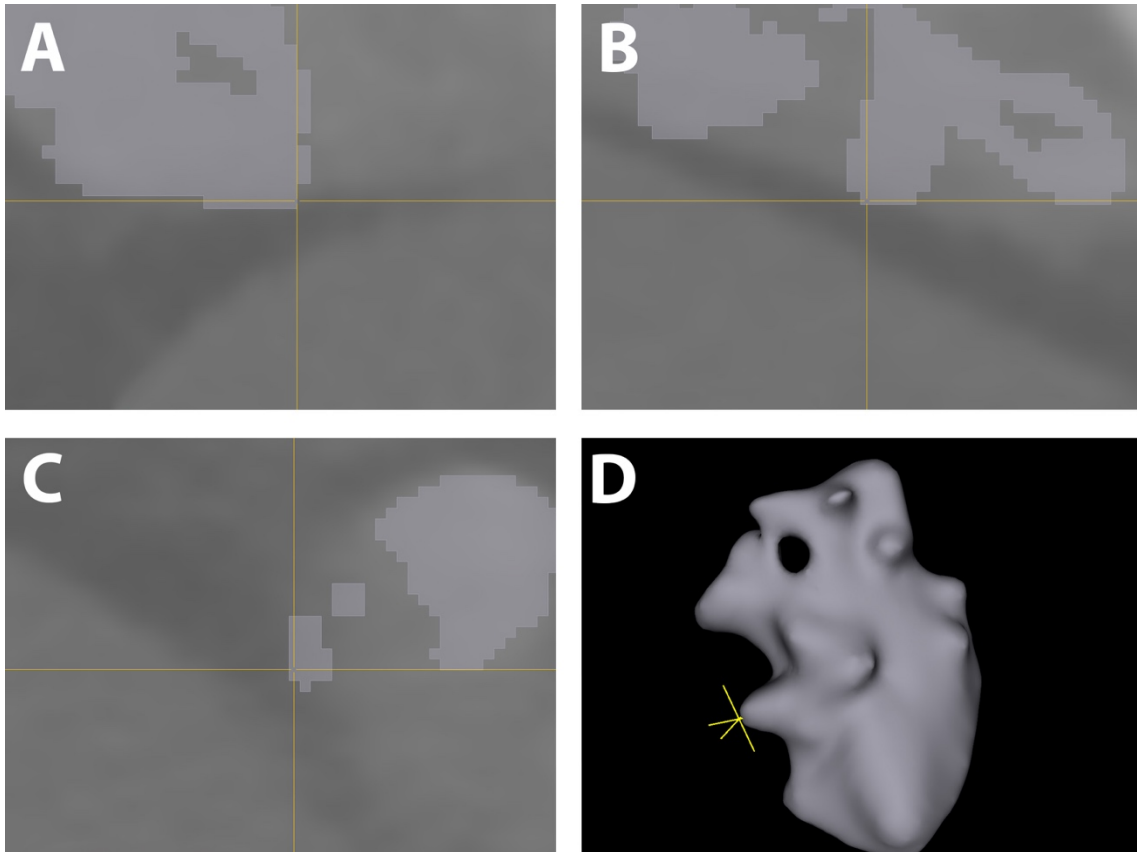
Figure 5. Volumetric calculation utilizing voxels: The yellow crosshair indicator aligns with a corresponding voxel in sagittal (A), coronal (B), axial (C) views, and the 3D model (D). Each voxel's resolution measures 0.744x0.744x0.744mm, equivalent to 0.412 mm^3. The tumor consists 126 504 voxels in total, therefore the volume is 52.12 cm^3.

3.2. METHODS – PART II: In-Silico Alignment of the Durable LVAD and Exoskeleton Production

3.2.1. Medical Imaging – CT Cardiac Angiography

CT images were made both before the implantation of the left ventricular assist device (within one month), and in the postoperative period (3-6 months following the implantation) (*Figure 6.*).
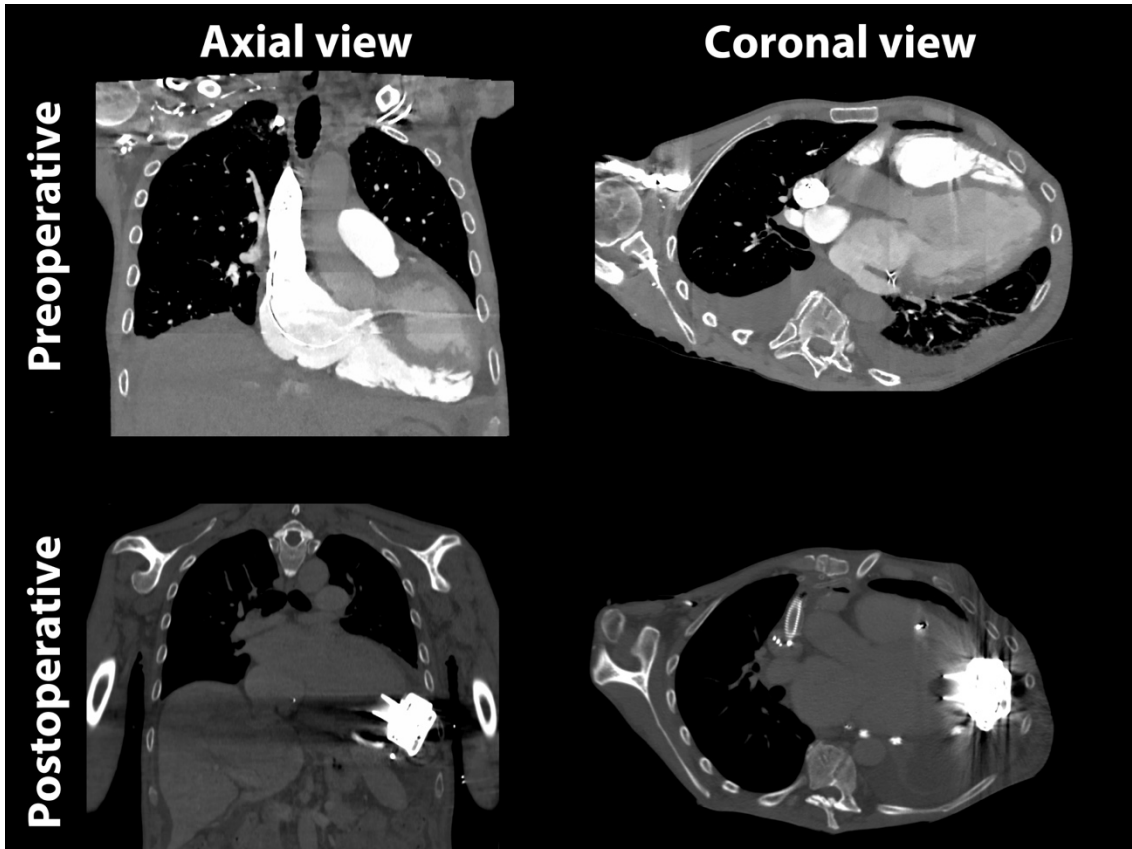
Figure 6. The preoperative and postoperative CTA images for the same patients were captured during the same diastolic phase.

ECG synchronized native and angiographic chest images were made in helical mode, with a 256-slice multi-detector CT device (Brilliance iCT, Philips Healthcare), using intravenous iodine contrast material, indexed to the body mass of the patients. Retrospective reconstructions were made of the series made with contrast material, as 10% regarding one R-R interval of the ECG registration. Thereby, a set of images encompassing the timeframe of a whole heart-cycle was created. For the planning phase, the images showing the end-diastolic state of the heart were used. The results we presented did not require additional CT scans; instead, we used CTA data from routine clinical use, which were required for other clinical aspects.

3.2.2. Heart Segmentation

The technique of image segmentation involves the creation of a binary labelmap for each anatomical component utilizing multiplanar CTA images. The process of semi-automatic surface segmentation encompasses the subsequent stages:

1. **Edge Detection:** The borders of the objects are outlined on 5-7 axial slices of the CTA dataset using a voxel-based intensity level tracing tool.

2. **Morphological Contour Interpolation:** Building upon the outlines from the previously generated labelmaps, the algorithm calculates labelmaps on intermediate slices by interpolating between manually drawn slices.

3. **Gaussian Smoothing:** A Gaussian method is employed to refine the outline of the binary labelmap.

4. **Shape detection:** The manual delineation of the mitral annulus and interventricular septum were made in cross-sectional axial CT images.

5. **3D planes definition:** The planes were established using the geometric distance from the contours of the mitral annulus and interventricular septal shape, ensuring that each contour point was equidistant from the respective plane.

The software utilized a real-time rendering technique to automatically build a 3D surface representation of a two-dimensional binary labelmap. The segmentation is exported as a 3D surface representation in the standard tessellation language (STL) file format.

Within the pre-existing labelmap of the heart, labelmaps are developed to depict the interior anatomical structures of the left ventricle, including but not limited to the interventricular septum, mitral valve, and papillary muscles. The technique of local thresholding segmentation is employed to generate a labelmap specifically for the left ventricular cavity. After performing intermittent manual adjustments and applying smoothing techniques, the labelmap corresponding to the left ventricular cavity is subtracted from the labelmap that encompasses the entirety of the heart. The segmentation procedure undergoes thorough evaluation by a multidisciplinary team comprising a radiologist, a cardiologist, and a cardiac surgeon. Any requisite modifications to the model are implemented in complete accordance with the clinical professionals.

3.2.3. Durable LVAD Anatomical Positioning

The DICOM-files, extracted from the angiographic CT-images were used to create the virtual geometry of the patient's heart. During the computational processing, or segmentation of the image data, functional units were marked off in the horizontal layers following each other. The individual steps of the segmentation and image-processing were described in our earlier publications (66). Following that, the segmentation of the myocardium and internal structures of the left ventricle (papillary muscles, mitral anulus and septum), due to their influence on the position of the inflow cannula, was done. Additionally, the pathological changes such as in cavity thrombus formation or post infarctional wall remodelling can also be visualized in the individual 3D model. In this personalized 3D model, the virtual left ventricular assist device is placed in such a way that the inflow cannula is placed in the optimal position (*Figure 7.*).
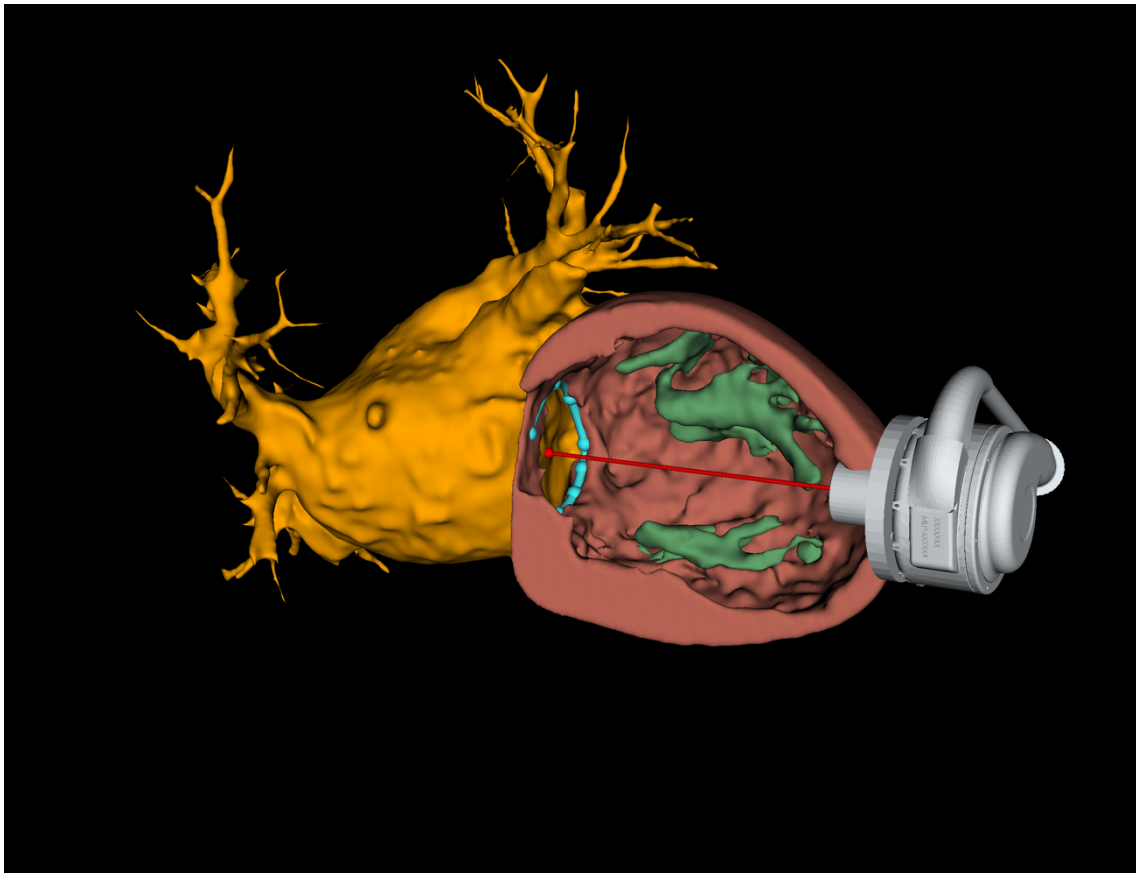

Figure 7. Anatomical positioning of the durable LVAD into the 3D segmented heart. Yellow: left atrium, blue circle: mitral annulus, red line: axis of the device directly facing to the center point of the mitral annulus, green: papillary muscles (47).

This process is called anatomical positioning, in which the position of papillary muscles, the thickness of the myocardium, the distance from the septum, and the individual geometry of the left ventricle are taken into consideration. The considerations regarding the anatomical positioning of the inflow cannula:

1. it has to be positioned in 0.5-1.5 cm parallel from the ventricular septum,
2. no obstacle should be formed by the papillary muscles or thrombi for the flow of blood, and
3. the inflow cannula is directly pointing toward the mitral valve centroid.

3.2.4. Functional Positioning with Computational Fluid Dynamical Simulations

In my thesis, the flow simulation setup was used based on Chivukula et al. work (9, 53, 71). Blood was modelled as a homogeneous Newtonian fluid using Navier–Stokes equations to simulate intraventricular flow pattern to determine the flow abnormalities:

$$\frac{\partial u}{\partial t} + u \cdot \Delta u = -\frac{\Delta P}{\rho} + \nu \Delta^2 u$$

where u is the fluid velocity vector, P is the fluid pressure, ρ is the fluid density, ν is the kinematic viscosity, and Δ^2 is the Laplacian operator.

The motion of platelet-surrogate particles was simulated. Over 1000 particles were individually tracked for each case, and particle trajectories were constructed to visualize the flow abnormalities inside the left ventricle.

All computational fluid dynamical (CFD) simulations were performed on FLUENT (ANSYS Inc., Canonsburg, PA) using second-order spatial and temporal formulation for the Navier-Stokes equations. All computations were performed on up to four 32-core nodes computer at Pázmány Péter Catholic University Faculty of Information Technology and Bionics.

The 3D model of the previously segmented heart was used for the analysis. Blood was treated as a non-Newtonian fluid, with a viscosity of 3.5 mPas and a density of 1050 kg/m^3. The hemodynamic parameters (turbulence) were measured quantitatively with different inflow cannula angles in the hydrodynamical simulation. The results were represented using a heat map. In the case of an inflow cannula with an inadequate

position, the unfavorable turbulent flow [30-80 m^2/s^2] is represented by color red. A favorable hydrodynamical state [2-22 m^2/s^2] is represented by the dominance of the colors blue, green and yellow.-In the latter case, the positioning of the inflow cannula was done with the optimal angle (*Figure 8.*).
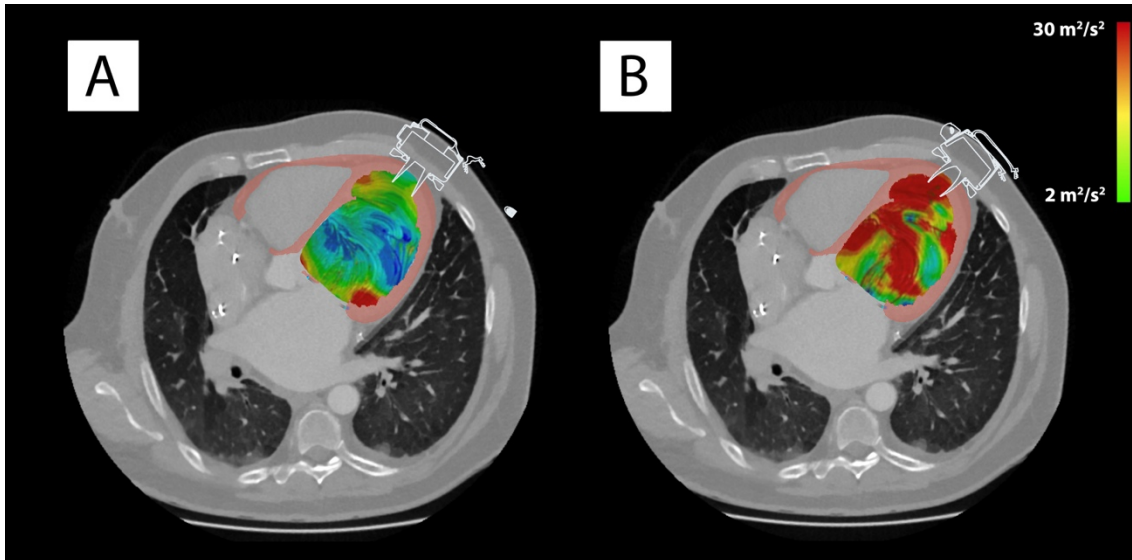

Figure 8. The impact of inflow cannula angulation on left ventricular flow patterns. The A presents the optimal flow pattern while the B shows the turbulent flow pattern due to the malangulation of the inflow cannula (47).

3.2.5. Design and Additive Production of the Exoskeletons

The Exoskeleton helping the positioning of the left ventricular assist device was individually designed in the virtual space, as an individual specimen, aligning to the position of the inflow cannula calculated during the 3D modelling and the hydrodynamic simulation. The Exoskeleton is perfectly fitted to the outer surface of the heart, incorporating the round opening positioned at the apex of the heart, which was designed to guide the coring knife. The *Figure 9.* shows the virtually fitted exoskeleton on the epicardial surface.
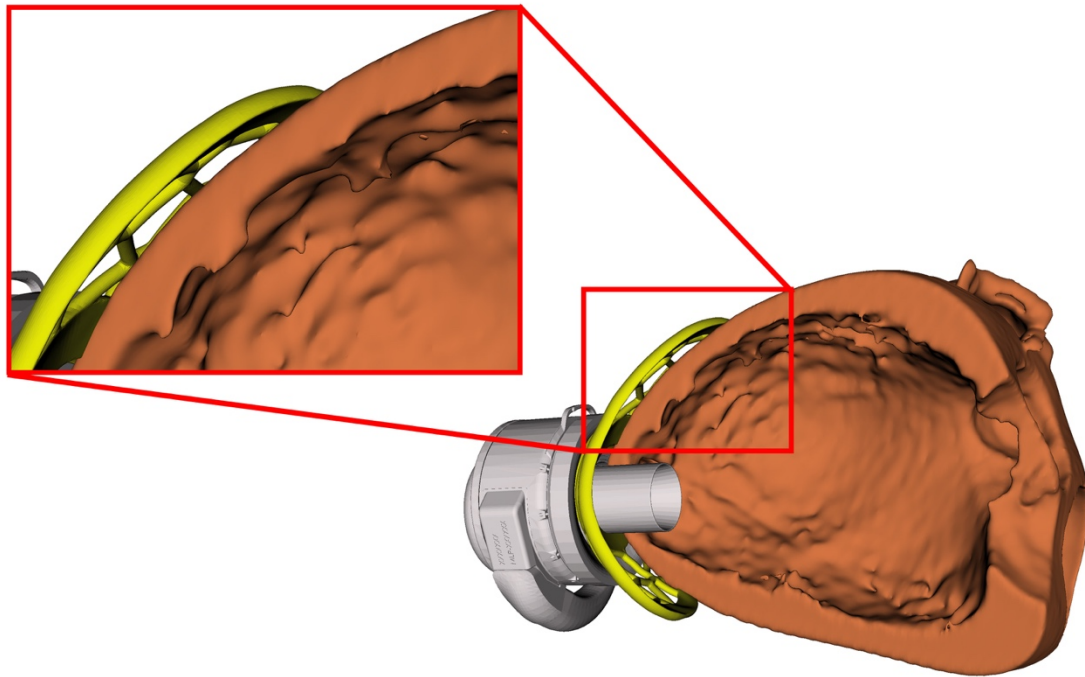
Figure 9. The Exoskeleton (yellow) accurately fits on the surface of the patient's virtual heart.

The positioning of the Exoskeleton can be fine-tuned using the left anterior descending coronary artery as a marking point guaranteeing that the 3D-printed model is exactly fitted to the surface of the heart, just like in the process of its virtual design. Using the Exoskeleton's guiding tube we could guarantee, that the inflow cannula was implanted in the previously designed position. *Figure 10.* shows the functional part of the Exoskeleton.
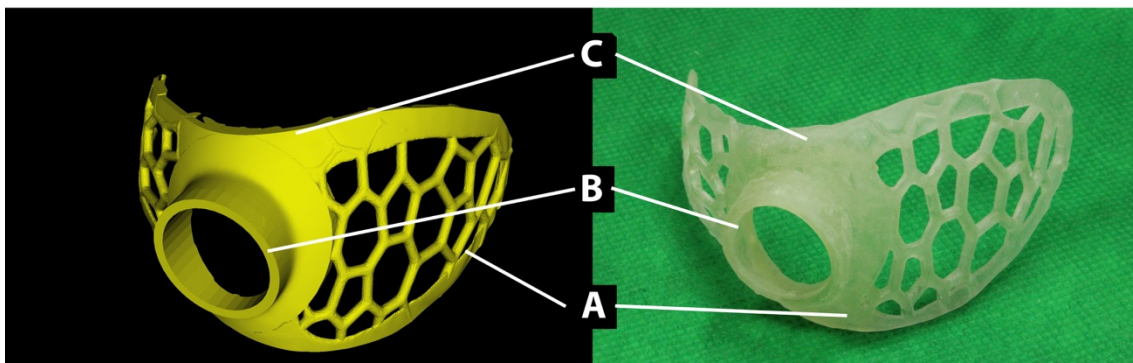

Figure 10. A: the skirt of the Exoskeleton. The concave surface accurately fits on the epicardium. **B**: The guiding tube designed for precise coring knife placement during the implantation. **C**: The septal edge of the Exoskeleton plays a crucial role in securing the correct position on the heart's surface, and the incorporation of a Voronoi pattern enhances surgical visualization during the coring procedure.

After the virtual design of the Exoskeleton, it was produced with medical-grade synthetic resin (USP class VI; ISO 10993-5-10-23), using 3D-printer (Formlabs 3B®, Formlabs, Somerville, MA, USA) stereolithographic rapid prototyping technology. *Figure 11.* displays the flowchart illustrating the modelling, printing, and quality control of the Exoskeleton.
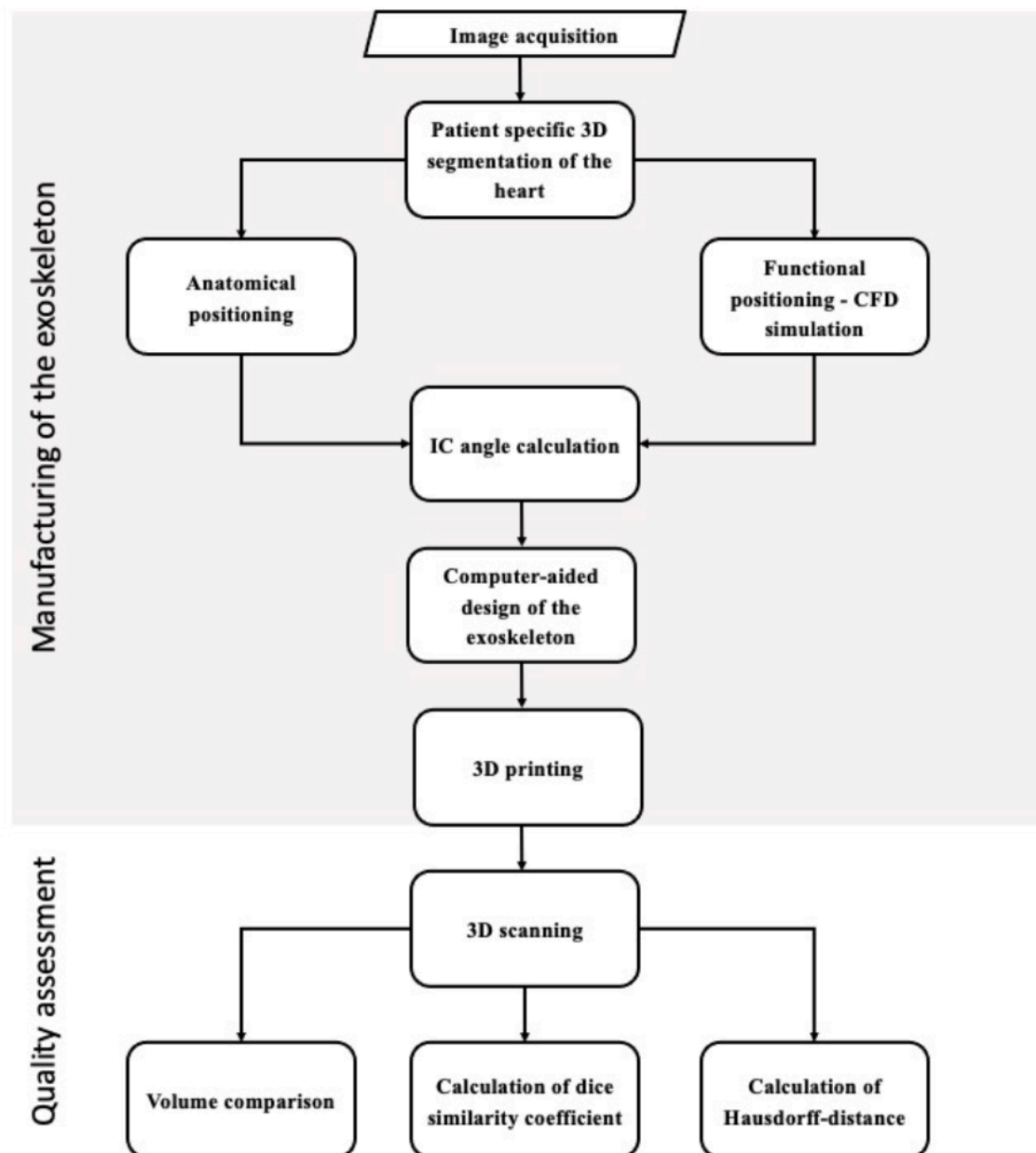

Figure 11. The flowchart shows the stages involved in the manufacturing and quality assessment process for the Exoskeleton (47).

3.2.6. Exoskeleton Quality Control

The quality control of the Exoskeletons produced through 3D-printing was executed by a 3D scanner (Einscan, Shining3D Technologies, China), by which high-quality point-clouds at 0.05mm single shot accuracy (ISO 12836) were emanated. The generation of colour deviation maps between the 3D printed Exoskeleton scanned STL and the master control file (original STL) was achieved using Geomagic Control X by 3D Systems (Rock Hill, SC, USA), a software developed for 3D inspection.

To assess the volumetric changes and surface quality differences, the 3D-printed Exoskeleton (3DPE) was scanned and compared to the master object, which represents the virtual 3D model of the Exoskeleton (VE). Dice similarity coefficient (DSC) and Hausdorff-distance (HD) were used for comparison the two models. These metrics were used to evaluate surface quality differences between the VE and 3DPE models.

The DSC (*Figure 12/A.*) serves as a reproducibility validation metric, quantifying spatial overlap between objects on a scale of 0 to 1. A DSC value of 1 indicates complete spatial similarity between two 3D models (78).

In contrast, the Hausdorff distance (*Figure 12/B.*) measures the distance between two sets of points, gauging the resemblance between superimposed objects. This distance offers three measurements on the models: (i) maximum distance between points, (ii) average distance, and (iii) the 95th percentile of distances measured (79).
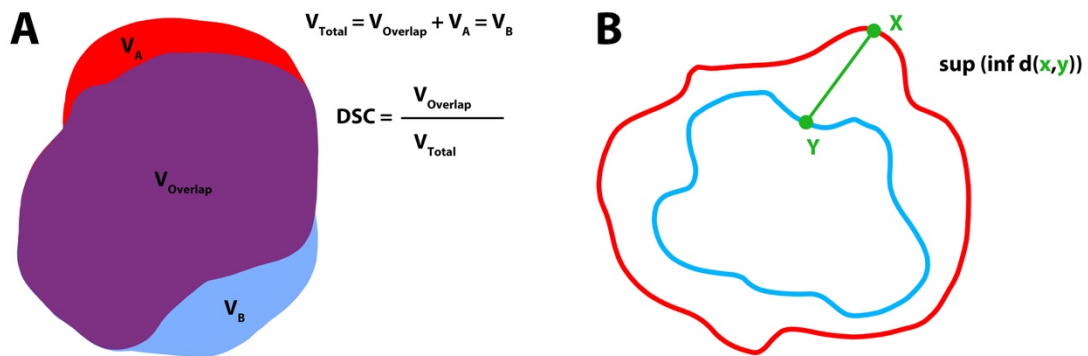

Figure 12. Visual representation of the Dice Similarity coefficient (A) and Hausdorff-distance meaning.

For both the VE and 3DPE to be considered identical, the DSC had to exceed 0.9, and the 95th percentile of the Hausdorff distance had to be under 1mm in all cases.

3.3. METHODS – PART III: Surgical Application and Postoperative Evaluation of the Exoskeleton

3.3.1. Study Design

The data sets of 57 advanced heart failure patients implanted with durable LVADs at Semmelweis University Heart and Vascular Center between 2015-2023 were analyzed. The research was conducted according to the requirements of the Declaration of Helsinki (80). The study protocol was reviewed and approved by the Local Research Ethics Committee (SE RKEB: 202-2/2005). Each participant was given written and verbal information regarding the process of the operation, and their clear intent of taking part in the study was expressed by written forms of consent. The patients were divided into two groups according to the method of the operation: (i) patients who were operated without navigation in the conventional way (control group, n=17), and (ii) patients operated with navigation, using preoperative planning, with the patented device (Exoskeleton) for the positioning of the inflow cannula (patent group, n=40).

3.3.2 Criteria for Patient Selection and Exclusion

Inclusion criteria were HeartMate III (Abbott, Plymouth, MN, USA) durable LVAD implantation due to advanced heart failure and signed consent for participation. Exclusion criteria were: (i) previous open-heart surgery, (ii) lack of CTA needed for the planning, (iii) lack of patient consent.

3.3.3. Propensity Score Matching

Biological sex, age, kidney function, end-diastolic left ventricular volume, previous infarction, and duration of postoperative inotropic medication were analyzed. In the process comparison, the method of pairing based on estimated probability of participation (Propensity Score Matching: PSM) was applied to the patient population of 57.

3.3.4. Surgical Application of the Exoskeleton

There was no difference in the surgical technique durable LVAD implantation was done with the same surgical steps in both groups, except the positioning of the left ventricular assist device, for which the Exoskeleton as a surgical navigation device was used only in the patent group.

In every case, the implantation of the left ventricular assist device was implanted after median sternotomy, with extracorporeal circulatory support. As the modelling was done based on CT-images made in the diastolic phase of the heart, the diastolic volume and geometry of the left ventricle was imitated, reducing the venous drainage of the heart (with sustained aortic inflow). The steps of the surgical application are shown on *Figure 13*. The positioning of the Exoskeleton to the apex of the left ventricle can be seen on *Figure 13/A*. The adequate position of the coring knife is precisely designated for the surgeon by the Exoskeleton fitted to the surface of the heart. In the next step, the coring knife is entered into the formed guiding canal (*Figure 13/B*). The implantation of the left ventricular assist device into the entry can be seen on *Figure 13/C*. The inflow cannula positioning is controlled with transesophageal echocardiography (*Figure 13/D*) that the next step is suturing the outflow graft to the ascending aorta (*Figure 13/E*). The drive line is pulled through the skin of the left upper quadrant of the stomach area. The implanted HeartMate III left ventricular assist device can be seen on *Figure 13/F*. The video of the implantation using an Exoskeleton can be watched in our publication (81).
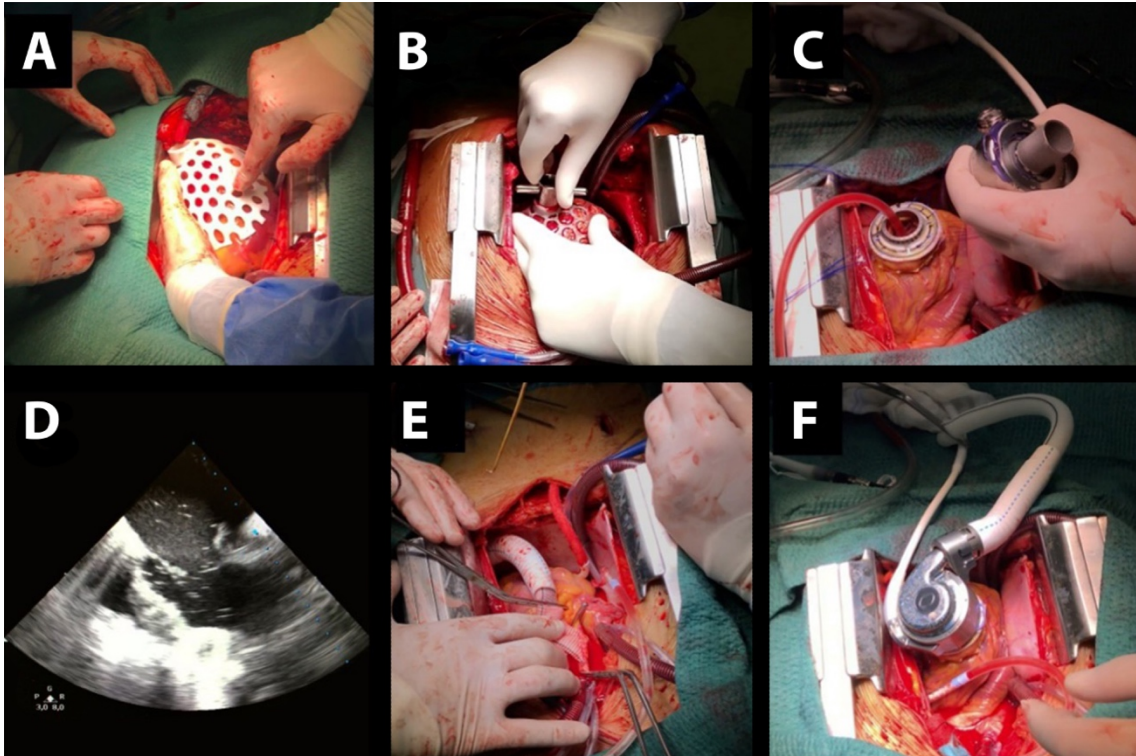
Figure 13. The steps of the surgical implantation [OH]: A: Placing the sterilized Exoskeleton on the epicardium, B: Guiding the coring knife into the Exoskeleton's channel, C: Implanting the durable LVAD, D: Monitoring the inflow cannula position with TOE, E: Suturing the outflow graft to the aorta, F: Completing the implantation (82)

3.3.5. Inflow Cannula Angle Calculation

The CTA imaging protocol is outlined in *Chapter 3.2.1.* The implantation angle derived from the coordinates of the computer-aided Exoskeleton. The segmentation was done using the individualized cardiac model focusing on the left ventricle and including the interventricular septum and mitral annulus. The device was virtually positioned within this 3D model, and the angle calculation in the preoperative period was straightforward, in postoperative CTA images the same calculation was performed. In *Figure 14.* the crucial components of the implantation can be seen such as the durable LVAD, the interventricular septum and mitral annulus and the papillary muscles. These structures were segmented using the method described in *Chapter 3.2.2.*
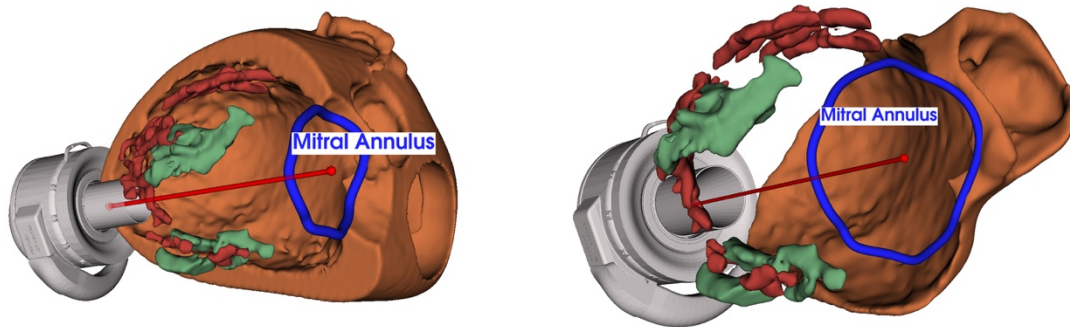
Figure 14. The preoperative positioning process of the durable LVAD. Light brown: myocardium and septum, Dark brown: trabeculae, Green: papillary muscles, Blue: mitral annulus, Red line: the axis between the LVAD and the central point of the annulus.

The angulation between the inflow cannula and the pertinent anatomical features, such as the mitral annulus and interventricular septum, required assessing the alignment between the axis of the inflow cannula and the plane defined by these anatomical structures.

The axis of the inflow cannula was determined by a line from the midpoint of the LVAD's base to the center of the inflow cannula. The mitral plane was defined as the equidistant surface points from the mitral annulus, while the septal plane was designed as equidistant surface points from the interventricular septum (*Figure 15.*).

The mitral angle calculation involved the computation of the angle between the IC axis and the mitral plane. Similarly, for the optimal septal angle, our calculations utilized the septal plane:

The direction vector ($\bar{s}$) of the IC axis:

$$\bar{s} = \text{Hiba! A könyvjelző nem létezik.},$$

where l and m are not both equal to zero.

The equation of the plane:

$$Ax + By + Cz + D = 0,$$

where A, B and C are not simultaneously equal to zero.

The angle (Φ) between the IC axis and the mitral or interventricular septum can be found using the following formula:

$$sin\ \Phi\ \frac{|A \cdot l + B \cdot m + C \cdot n|}{\sqrt{A^2 + B^2 + C^2} \cdot \sqrt{l^2 + m^2 + n^2}}$$

In the postoperative CTA images, the methos was the same as in preoperatively. The durable LVAD was placed regarding its postoperative CTA coordinates (*Figure 15.*).
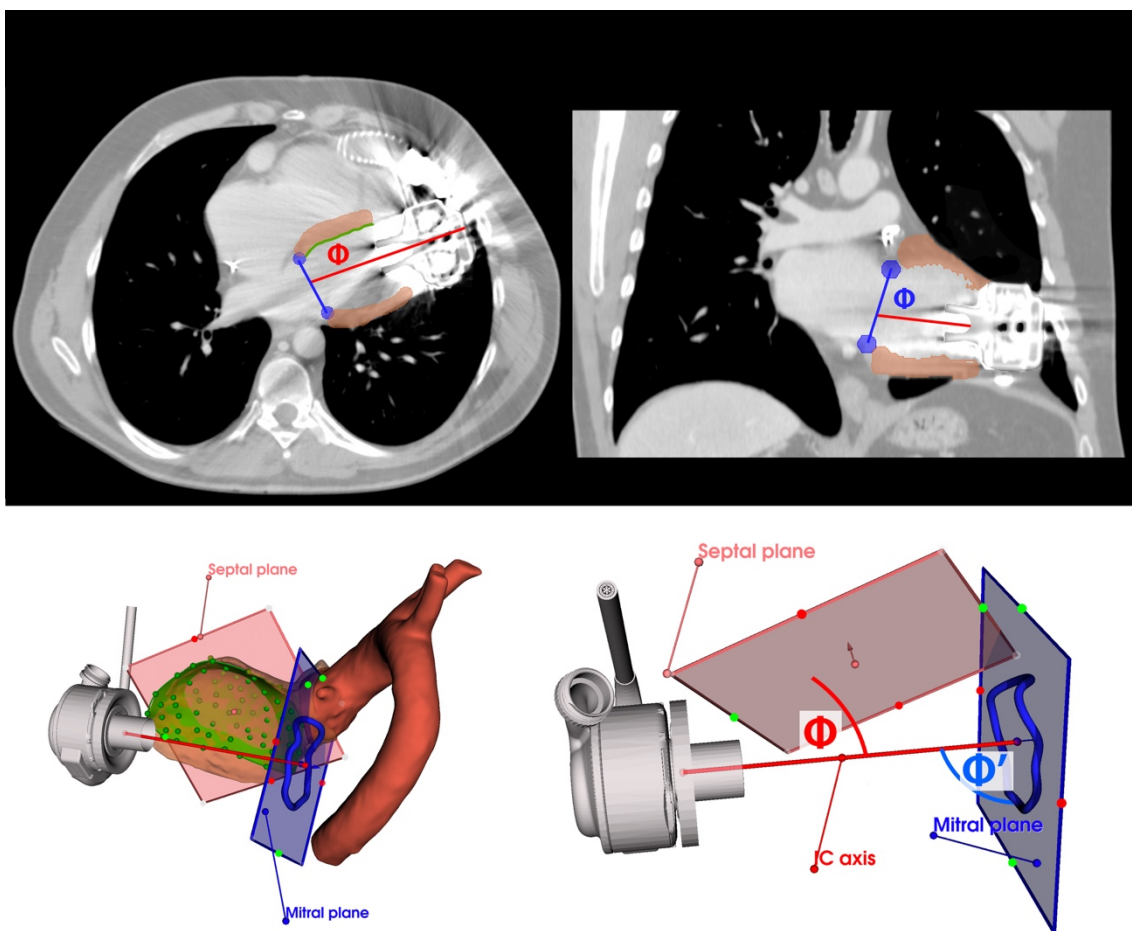

Figure 15. The calculation method of the inflow cannula in relation with the interventricular septum and the mitral annulus plane. The Φ (red) is the angle between t the axis of the inflow cannula (red line) and the interventricular septum (green). The Φ' (blue) represents the angle between the inflow cannula and mitral annulus (blue plane).

4. RESULTS

4.1. RESULTS I: Model Accuracy measurements

In 2019, our research group investigated the accuracy the 3D modelling methods using solid tumor volume (66). The evaluation of model accuracy was based on the comparison between the intended and observed characteristics, including the location, shape, and volume of the excised tumors. A total of 18 tumor instances were subjected to 3D design for the purpose of comparison, out of which 11 were subsequently printed. The anticipated position, configuration, and spatial alignment of the tumors relative to the adjacent structures were in accordance with the observations made during the surgical procedure. The volumes exhibited no statistically significant disparities. The average volume of the simulated tumors in the group that underwent 3D modeling was found to be 56.21 ± 19.61 cm^3, while the observed volume of the tumors during pathological processing was 53.11 ± 21.61 cm^3. There was no statistically significant difference seen between the two groups (p = 0.7188, Paired Samples t Test, *Figure 16.*).
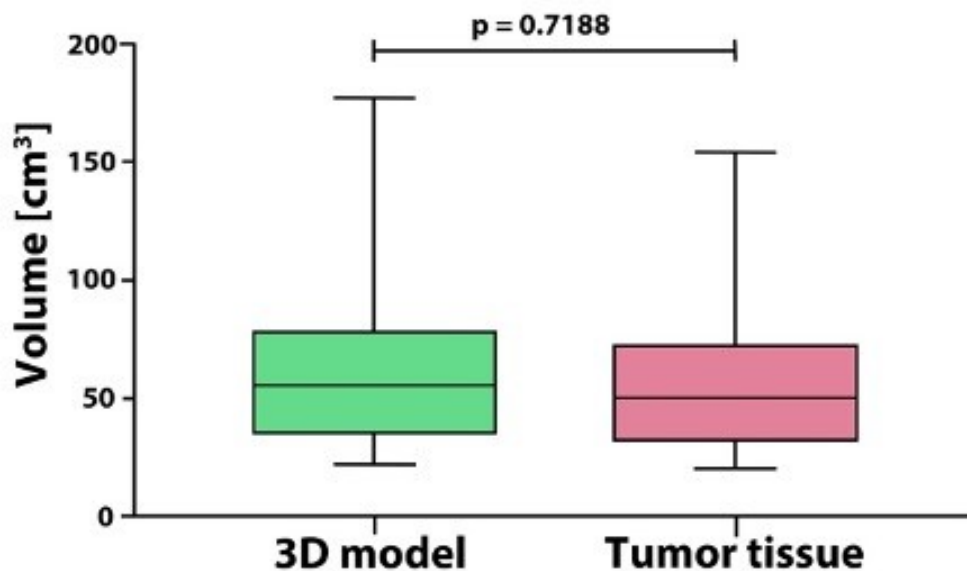

Figure 16. Comparison between the 3D predicted volume and the pathologically observed volume. The volumes do not differ significantly from each other, it ensures the modelling accuracy for our following studies (66).

Consequently, the efficacy of our 3D segmentation and modelling technique was found to be satisfactory, thus rendering it suitable for subsequent 3D modelling endeavors. In addition, these models have the potential to serve as a valuable tool for surgical decision making.

4.2. RESULTS II: Design and Quality Control of Exoskeleton

4.2.1. Exoskeleton Computer Aided Design

The Exoskeleton was designed to fit the outer surface of the apex of the left ventricle, used MATLAB software, which was capable of free-form surface modeling (*Figure 17.*).
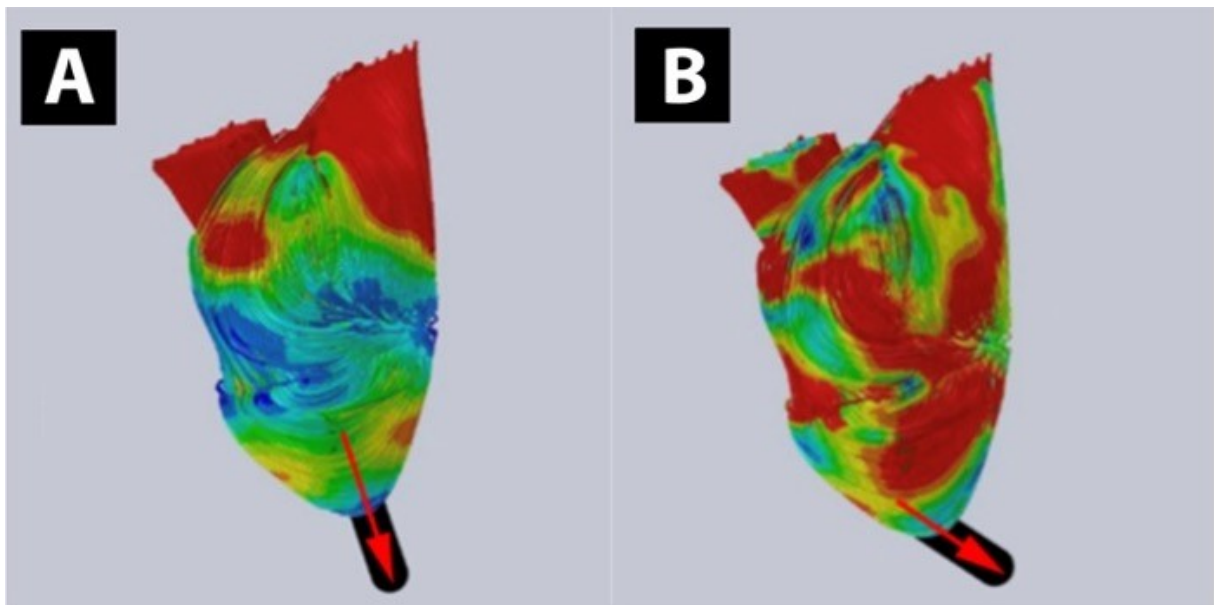

Figure 17. The Exoskeleton is tailored to the surface of the patient-specific heart model, ensuring accurate placement of the IC during the implantation (47).

This design, based on the heart model generated from CTA scans, ensures a precise fit during surgery. To facilitate the surgical usability during the implantation, the Exoskeleton's size is preserved as minimal as possible while providing reliable support for guiding the coring knife—used to cut a cylindrical section of the heart muscle for the inflow cannula implantation. The surgical instruments and the implantation steps are described in *Chapter 3.3.4.*

The Exoskeleton base takes on a leaf-like shape from the heart's apex to the IVS, incorporating a cylindrical guide channel for the coring knife. This guiding channel, housed within the Exoskeleton base, directs the knife, securing the planned placement of the LVAD. The Exoskeleton's skirt is further refined using a Voronoi-pattern, ensuring the clear vision of the epicardial surface. Once the design is finalized, the model of the Exoskeleton is exported as a standard tessellation language (STL) file and prepared for 3D printing and quality control.

4.2.1. Volume quality comparison

Original Exoskeleton-volumes were measured to be 10810.39mm^3 ± 1692.01mm^3; 3D printed, and back-scanned models were found to be 10805.07mm^3 ± 1700.97mm^3. No significant difference was found between the volumes (p= 0.7582). The mean of differences between the master scan and the scanned 3D printed models was measured to be - 0.54 ± 52.32 mm^3 (*Figure 18.*).
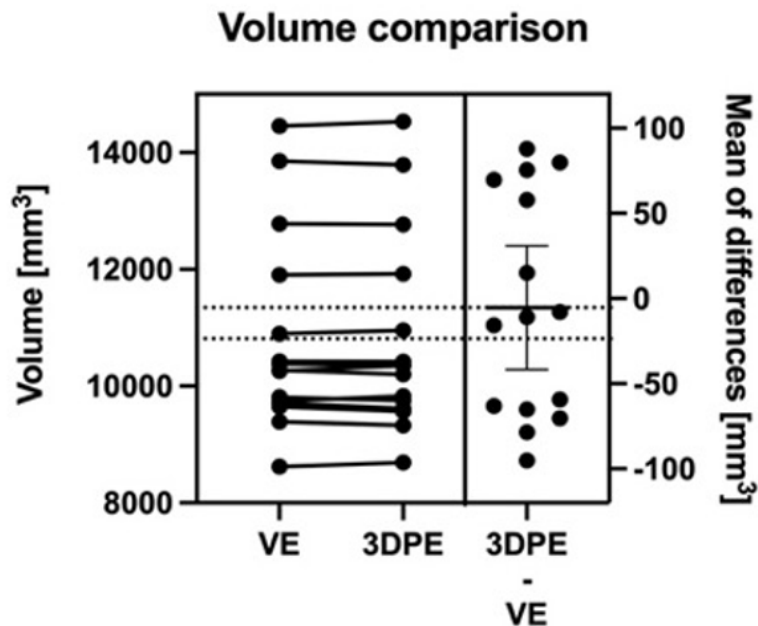

Figure 18. Volume and mean of differences comparisons between the virtual Exoskeleton (VE) and 3D printed Exoskeleton (3DPE) (47)

4.2.3. Surface Quality Comparison

The maximum, median, and 95th percentile Hausdorff-values were all recorded for the virtual and printed Exoskeleton comparison dataset. The maximum values were found to be within a range of 2.83mm ± 1.31mm, with a mean of 2.17mm ± 0.52mm. The average distance mean was measured to be 0.16mm ± 0.06mm. In each of the 3D scanned Exoskeletons, the 95th percentile of the distance was found to be under 1mm (0.6mm ± 0.21mm), with a 0.31mm minimum distance, and a 0.94mm maximum distance. The Dice similarity coefficient and Hausdorff-distance parameters are presented in *Table 3*.

	Dice Similarity Coefficient	**Hausdorff-distance**		
		Max [mm]	*Average [mm]*	*95% [mm]*
Maximum	0.98	2.83	0.26	0.94
Minimum	0.91	1.31	0.08	0.31
Mean	0.95	2.17	0.16	0.60
Standard Deviation	0.03	0.52	0.06	0.21

Table 3. *Surface quality comparison between the original STL file and the 3D printed and back scanned models (47)*

We created a deviation map to visualize the surface similarity data. In the deviation map, the colours yellow, we used orange and red to describe areas with negative material discrepancy, while blue and cyan to describe areas with a surplus of material in comparison with the original STL object. No considerable differences were present between master and back scanned Exoskeleton objects in *Figure 18*. A distance inequality of over 1 mm is revealed only at the edges of the Exoskeleton, at a maximum value of 2.83mm. Meanwhile, the average 95th percentile of two points distance was found to be 0.60mm, a value substantially under the accepted 1mm distance difference.
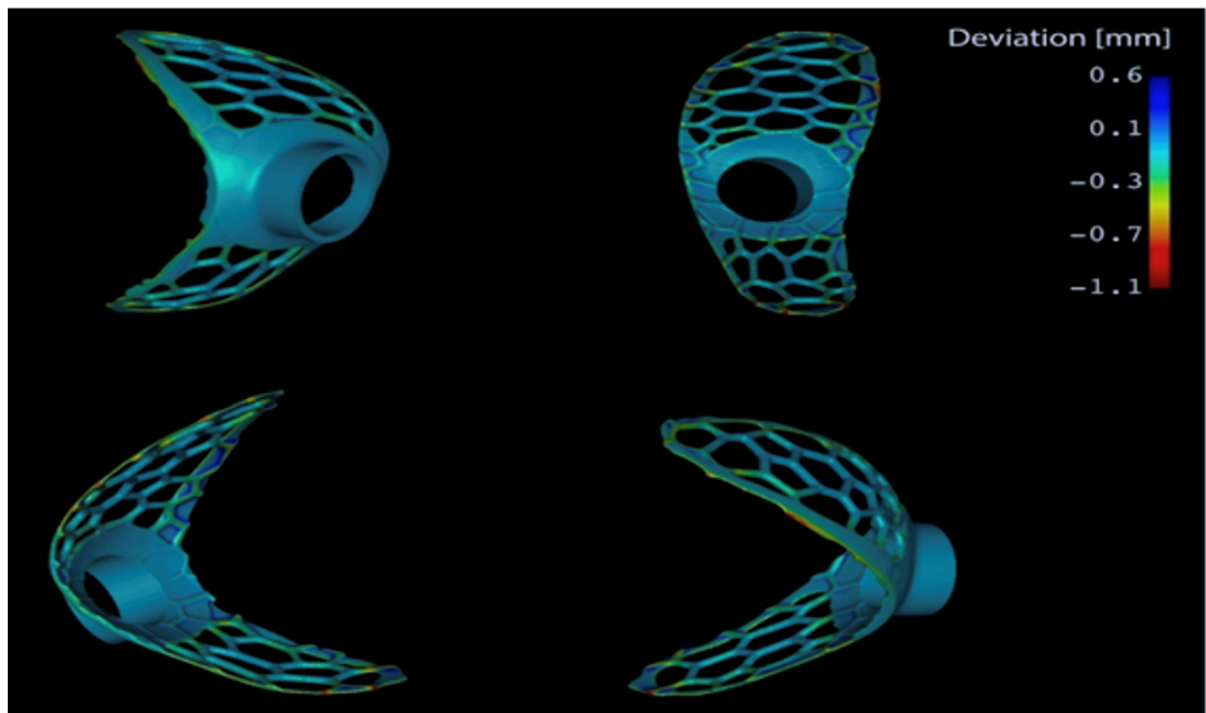
Figure 18. The deviation map shows the differences between the original STL, and the back scanned 3D printed Exoskeletons (47)

4.3. RESULTS III: Exoskeleton Utilization in Clinical Practice and Post-Implantation Assessment

4.3.1. Patient Characteristics

14 patient data were compared using PSM calculation. The success of the pairing is shown in *Table 4.* The PSM value of the patent group was found to be 0.524, while the PSM value of the control group was measured to be 0.531. Regarding the risk factors, both groups were found to be homogenous.

	PSM Results	Patent Group	Control Group before PSM ▲	Control group after PSM ◆
	Tabel 4. The effectiveness of the propensity score match is depicted by the vertical line. The correlation is stronger if the data of the group align with the 0 point. Following the pairing, the differences were not significant between the patent group and the control group (82).			
Propensity Score			0.524	0.005
Sex [male]		84%	78%	84%
Age [yesr]		61.8 ± 3.7	65.6 ± 4.1	60.5 ± 3.2
Kidney Function [ml/min]		97.03 ± 12.2	86.61 ± 18.4	96.12 ± 10.34
LVEDV [ml]		151 ± 17.8	160 ± 41.7	152 ± 21.6
Previous Infarction		16.7%	24.4%	16.7%
Inotrope dependency		0%	9.75%	0%

The mean age of the patients in the patent group was 61.8 years ± 3.7 years on average, and in the control group it was 60.5 years ± 3.2 years. The proportion of biological sexes were equal in both groups (1:6 = women: men). Renal impairment could not be diagnosed in either group (97.03 ± 12.2 vs. 96.12 ± 10.34 ml/min derived creatinine clearance). One previous myocardial infarction was identified (14.3%) in both groups.

4.3.2. Inflow Cannula Angulation Measurements

During the evaluation of the post operative CTA images, the angle closed by the inflow cannula and the interventricular septum in the patent group was measured 10.13º ± 2.69º, and in the control group, it was found to be 22.87º ± 12.38º on average. As a result of Student T-test, a statistically significant difference between the average results of the two groups was found (p=0.0208). In both groups, the average results were within normal range as described in the relevant literature. In four cases of the control group (n=4), a higher deviation in post operative angles than in the literature was identified, where the maximal deviation was found to be 34.60º.

4.3.3. Flow Pattern Differences between the two Groups

There was a significant difference in turbulence between the two groups during CFD simulation (*Figure 8. and Figure 17.*). Simulated turbulent kinetic energy was measured

significantly lower on average in the patent group ($11.7 \text{ m}^2/\text{s}^2 \pm 9.39 \text{ m}^2/\text{s}^2$), compared to the results of the control group ($49.59 \text{ m}^2/\text{s}^2 \pm 7.61 \text{ m}^2/\text{s}^2$ on average).

Left ventricular end diastolic volume was not found to be significantly different between the two groups. The starting left ventricular end diastolic volume was $149.1 \text{ ml} \pm 37.3 \text{ ml}$ on average in the patent group, while it was shown to be $151.6 \text{ ml} \pm 12.17 \text{ ml}$ on average in the control group (p= 0.8697), however post operatively, a significant difference was identified between the results of the two groups (p= 0.0302). Left ventricular volume decreased in both groups. Post operative end diastolic volume was $139.11 \text{ ml} \pm 9.80 \text{ ml}$ in the control group, while it was $116.94 \text{ ml} \pm 21.77 \text{ ml}$ in the patent group.

5. DISCUSSION

Our research project began by using 3D technology to reconstruct left ventricular aneurysms (83). This was achieved through the implementation of computer-assisted ventricular engineering (CAVE), which involved indexing the post-operative left ventricular volume to the patient's surface area. CAVE facilitated the development of patient-specific, computer calculation supported surgery. This cutting-edge approach enabled the development and refinement of subsequent 3D methodologies in the presented research work.

Our first 3D printed model was performed in a case of aortic pseudoaneurysm in a 55-year-old female patient after a Bental procedure in 2016 (84). This first model demonstrated the clinical advantages of using 3D models, especially in complex anatomical scenarios.

Our research aligns with the findings of Shi L. et al. (85), who found that 70% of clinicians expressed an interest in employing 3D technology within their medical practice and concluded that the average accuracy of individually created 3D models exceeded that of conventional CT-generated models. Additionally, a systematic review published in the Journal of Surgical Education in 2018 described the usage of 3D printed models in surgical training and postoperative results evaluation. The utilization of 3D models in clinical practice resulted improved postoperative outcome (86). Yang et al. (87) conducted a retrospective cohort study to assess the efficacy of patient-specific 3D printed models in preoperative planning for corrective surgery for patients with idiopathic scoliosis. The study analysed 126 cases, of which 50 patients were operated using 3D printed spinal models, while 76 were operated without 3D printed models. The research displayed statistically significant decreases in operating time, blood loss, and transfusion volume in the perioperative setting ($p < 0.001$) in cases 3D model was used. In addition, a study by Liu et al. (88) indicated that using patient-specific 3D models generated from CT scan data resulted in a 20% decrease in operating time.

Over time, our research group extended to encompass thoracic and paediatric cardiac surgical specialties. Our study in 2019 aimed to investigate the surgical applications of 3D technology, with a specific focus on Hungary (66). The research involved the

assessment of 121 virtual models, 49 of them were 3D printed. It provided detailed demographic profiles of patients who underwent 3D modelling, as well as insights into imaging modalities, diagnoses and 3D printing methodology. 10.2% (n = 5) of the cases were related to thoracic surgery, and 89.8% (n = 44), were in relation to cardiac surgery. The median age of our patients was 49.7 years, with 57.1% (n = 28) of the cohort being males. We also concluded in our research the 3D virtual and printed models' advantages in preoperative planning, highlighting their role in reducing bleeding and operation time. Our findings suggest that virtual 3D models can be translated into personalized, life-sized 3D printed models, providing enhanced anatomical context compared to standard 2D radiologic images. These models aid in precise measurements and planning stages of surgery.

Our study evaluates the accuracy of 3D models concerning the intended and observed parameters of surgically excised thoracic malignancies. Of the 18 tumour cases examined, 11 were replicated by 3D printing, revealing an alignment between the 3D planned and observed spatial associations with no significant differences in tumor, position and size. Additionally, it should be noted that there was no significant difference in tumor volumes observed between planned and actual measurements (51.12 ± 23.3 cm3 versus 49.74 ± 21.9 cm3, p = 0.7188).

Our experience is characterised by the approach integrating 3D technology into clinical practice. In 2014, our first utilisation of 3D technology during surgical procedures, as cited in (83), supported us to enhance surgical interventions. Thereafter, in 2019, our continued efforts to advance medical technology led us to embark on a significant investigation. This research aimed to evaluate the accuracy of our previously developed 3D modelling methodology. Our objective was to validate and confirm the precision of this technique, and enhancing its reliability. In addition to verifying the precision of our 3D modelling approach, this study established its safety and efficacy in patient care, ultimately laying the foundation for its clinical implementation (66).

In recent years, our research team developed a growing collaboration between different clinical specialties involved in several 3D medical projects. This collaboration gained significant momentum when Béla Merkely, the rector of Semmelweis University, established the 3D Centre on the university campus in October 2020. This center was

specifically designed to facilitate the widespread integration of cutting-edge technology into ongoing research, educational programs and patient care.

The fundamental mission of the Semmelweis 3D Centre focuses on the proactive incorporation of novel technologies into multiple dimensions of medical practice and its relentless pursuit of advancement. The current program of the Semmelweis 3D Centre includes three undergraduate courses and one postgraduate course. These courses have been carefully designed to explore the complex intersection of medical and engineering studies, placing particular emphasis on the complexities of 3D modelling and printing technology.

Within this academic context, our students are presented with an array of invaluable opportunities to actively engage in a range of clinical projects. The students undertake the complex task of modelling complicated surgical scenarios, gaining a wide range of detailed clinical experience from accurately planned cases, thus enriching their educational journey.

Simultaneously, the Semmelweis 3D Centre maintains strong connections with eight clinical departments, fostering synergy between academia and healthcare practice. *Table 5.* highlights the wide range of ongoing projects at the Semmelweis 3D Centre, demonstrating the extensive research and innovation being carried out.

Table 5. The Semmelweis 3D Center clinical cooperations	
Name of Institution	**Project Name**
SU- Heart and Vascular Center	Exoskeleton
SU - Department of Thoracic Surgery	Vasculature visualization in lung tumor
SU - Department of Surgery, Transplantation and Gastroenterology	3D based decision making support for living donor kidney transplantation
SU - Medical Imaging Centre	AI based segmentation method development
SU - Peadiatric Surgery	Patient-specific 3D reconstruction in straight back syndrome cases
Gottsegen National Cardiovascular Center - Congenital cardiacsurgery	Preoperative 3D modelling decision in complaex anatomical situations
National Institute of Oncology - General Surgery	Mesenteric vein visualization in right side hemicolectomy
National Institute of Oncology - Radiology	Radiomic feature analysis in segmented tumor models

After validating the accuracy of 3D modelling and advancing 3D technology, a critical challenge for both surgeons and patients emerged in durable LVAD positioning. It has previously been acknowledged that improper placement of the inflow cannula can lead to device malfunction, compromising tissue perfusion and contributing to a low output state associated with hemodynamic instability (89). The installation of a durable LVAD

intricates and requires careful attention. It is commonly performed in specialist high volume institutions. These centres have been found to have lower rates of postoperative problems such as haemorrhage, infection, right ventricular failure, and mortality (90). However, the absence of exact device placement can lead to large variations in outcomes, even when performed by a skilled surgeon. Improper placement of the inflow cannula might result in adverse dynamics of ventricular blood flow after surgery, hence increasing the risk of thromboembolic events in both the short and long term. It is important to highlight that the challenges emerging from device malposition can be effectively addressed or completely avoided by employing the exoskeleton.

Chivukula was one of the pioneers who calculated the ideal angle for the inflow cannula in the left ventricle (9, 53, 71). Using computational fluid dynamics simulations, Chivukula demonstrated a significantly increased risk of thromboembolic complications and an increased long-term susceptibility to micro emboli formation, causing stroke, in inadequate positioning of the inflow cannula. Chivukula also identified and stated three key factors that contribute to post-operative complications.

Firstly, it has been found that global geometry and ventricular size have an independent risk of ventricular assist device thrombosis. According to a previous study, left ventricle chamber size and geometry have a significant impact on the hemodynamic profile (71). In patients with smaller left ventricles using durable LVADs, the flow pattern triggered platelet activation and promoted thrombus formation, significantly increasing device thrombosis and neurological events (71).

Secondly, the depth of the inflow cannula insertion was revealed to be a critical factor increasing the risk of post-operative thrombosis. The extent to which the inflow cannula is inserted within the ventricle cavity has a significant impact on the flow of blood in the left ventricle. Deeper insertion can increase platelet deposition almost fourfold, thus increasing platelet activation, thrombosis and the risk of stroke (9).

Finally, the suboptimal hemodynamic changes in the left ventricle after implantation could also happen by malangulation of the inflow cannula (53). The ideal angle for the inflow cannula was $0\pm7°$ from the left ventricle apical axis to the mitral annulus. In this range, the flow pattern was optimal and there was a significant reduction in the risk of thromboembolic complications. Out of this angle, the rate of postoperative complications

increased. The research established that aligning the inflow cannula with the central point of the mitral annulus could reduce post-operative complications.

Several other studies conducted that life expectancy of patients with a left ventricular assist device was reduced by the misplaced inflow cannula (12, 54, 89).

An unfulfilled clinical demand was evident, which established the ideal parameters for durable LVAD placement and inflow cannula positioning within the left ventricle based on basic science. Our 3D modelling method offered a possibility to generate precise, patient-specific 3D models that include all relevant cardiac structures that influence the placement of the inflow cannula and postoperative outcomes following durable LVAD implantation.

Subsequently, a 3D model of the heart was created for each individual patient, allowing in silico positioning of the durable LVAD device. This approach allowed accurate control of important parameters that affect post-operative outcomes, including the depth of the inflow cannula, its relative position to the interventricular septum and papillary muscles, and its alignment with the mitral annulus.

This innovative approach was the first in the world to control each variable with a personalized decision support system for implantation.

The developed new surgical device -called exoskeleton- was a surgical guide customized to fit accurately on the epicardial surface of the left ventricle containing an integrated guiding tube to orient the coring knife, thus securing anatomical placement and orientation of the inflow canula to prevent post-implantation occlusion by internal cardiac structures such as papillary muscles or intraventricular thrombus.

As a result, the inflow cannula faced to the central point of the mitral annulus runing parallel to the interventricular septum, resulting an optimal blood flow patterns within the left ventricle after implantation, thus significantly reducing complications associated with cannula misalignment. The 3D-printed exoskeleton was made from sterilizable surgical-grade material, designed for intraoperative use on the surgical field.

The first clinical application of the exoskeleton was published as a state of the art in 2019 (81). In this instance, we conducted a validation process to assess the precision of LVAD placement. This was achieved by comparing the angulations between the interventricular septum and the inflow cannula on both the preoperative plan and the postoperative control

CT scan. The discrepancy between the intended and observed placement of the inflow cannula was measured 2.6°.

Our innovation was submitted to the patenting procedure in Hungary (91) and internationally (92), the patent applications were completed in 2019. These patent applications were officially filed in 2022.

In our 2023 published trial, we performed durable LVAD implantation in a carefully selected cohort of seven patients. The patented group underwent guided LVAD implantation utilizing 3D technology, while the control group underwent conventional implantation without the aid of navigation. We investigated the angle at which the inflow cannula was positioned relative to the interventricular septum as the primary variable in our research. Additionally, we examined the flow characteristics of the left ventricle following the placement of a LVAD.

After the implantation procedure, a significant difference in the angle of the inflow cannula was observed between the group of patients (10.13° ± 2.69°) and the control group (22.87° ± 12.38°), which was statistically significant. It is important to note, however, that the mean values for both groups were within the accepted angle range. The fourfold variability observed in the standard deviation values, however, indicates that the use of navigation during surgery leads to improved reproducibility of results. The reason behind this is that traditional positioning is predominantly influenced by human factors, whereas implantation utilizing exoskeleton is not subject to such biases. During the study, the LVAD was surgically implanted equidistant from the anterior and posterior papillary muscles. According to current evidence, this factor can only be considered when using the exoskeleton.

The decrease in left ventricular end-diastolic volume was significantly greater in the patent group after the implantation. This has been attributed to the favourable placement of the inflow cannula in the left ventricle. The left ventricular volume can more efficiently pass through the inflow cannula without any blockage due to its almost parallel angle to the interventricular septum and equal distance from the papillary muscles (93). The concept is supported by the observation that turbulence levels in the left ventricle during flow simulations were significantly lower in the patent group (mean: 11.76 m^2/s^2 ± 9.39 m^2/s^2) compared to the control group (mean: 49.59 m^2/s^2 ± 7.61 m^2/s^2).

Based on our clinical experience and preliminary results, the integration of exoskeleton technology could have a potential to reduces the misplacement of the durable LVADs, resulting in consistent, predictable surgical outcomes. We also showed, that our exoskeleton system could enhance the surgeon's understanding of the patient's anatomical situation, especially helping to identify the relationships between anatomical structures. This proved beneficial in complex anatomical scenarios where direct visualisation is limited. The opportunities for 3D modelling and printing technology in the medical field are considerable. They facilitate preoperative surgical planning, providing detailed preparation prior to surgery. Our ongoing research has received favourable feedback from surgeons, validating the efficacy and value of this technology. However, the limited access to technical expertise, including proficiency in diverse software, 3D modelling and printing techniques, post-processing protocols, and the availability of 3D printers, presents a significant limitation to widespread integration into routine clinical practice.

The advantage of our method is the possibility of standardisation of durable left ventricular assist device implantation with the exoskeleton offering the potential to avoid complications arising from improper positioning of the inflow cannula, such as cannula obstruction due to the interventricular septum or papillary muscles and unfavourable left ventricular flow pattern. Additionally, the postoperative deviation of the inflow cannula angle is smaller and therefore more predictable than other implantation techniques. Furthermore, this technique has the potential to decrease operating time, providing a personalised and more safe surgery.

The disadvantage of our technique is the considerable time required for the planning phase, as well as the extensive understanding of radiographic image processing, computer calculation, 3D modelling and 3D printing. In addition, the segmentation and 3D modelling of the exoskeleton, still require significant human interaction.

The study's small sample size was a significant limitation, it also has to be recognised that clinical variables such as stroke, systemic embolization, length of intensive care unit and hospital stay are influenced by multiple factors. While the inflow cannula's left ventricle positioning is important, it is not the sole determinant of postoperative outcomes.

The future improvements could be the automatization of the exoskeleton production, and using advanced deep learning segmentation algorithms and dedicated software for angle calculation in the post-operative evaluation. Through these improvements has the

potential to improve the planning phase and reduce the occurrence of sporadic errors caused by human intervention. Additionally, our goal is to establish the efficacy of our patented technology through a randomised controlled trial.

6. CONCLUSION

I. Our research provides an improvement in left ventricular assist device implantation, addressing critical challenges through innovative technology and methodology. By utilizing clinical 3D modelling using DICOM imaging data, we've developed anatomically accurate models that are critical for accurate prediction of tumor volumes (66). Furthermore, the establishment of the 3D Centre at Semmelweis University under the supervision of Béla Merkely, the Rector of the University has strengthened our commitment to research, education and patient care.

II. Our achievements included the development of a novel approach to durable LVAD inflow cannula positioning. Using personalised 3D models, we created the exoskeleton (47) – a surgical tool that could facilitate intraoperative navigation during LVAD implantation (81). Our comprehensive evaluation confirmed the efficacy and demonstrated the ability of the exoskeleton to provide reproducible and consistent implantation, as demonstrated by post-operative evaluations that highlighted the exoskeleton's results in achieving predictable outcomes (82). Our method has been recognised globally and secured patents in Hungary (91) and internationally (92). The engineering-based evaluation confirmed the precise volumetric and surface accuracy of the 3D printed comparing with the virtual exoskeleton, which ensured its safety and efficacy in clinical application.

III. The clinical validation in our research revealed the alignment between the planned implantation angles and post-surgical outcomes, emphasising the reliability of our approach (82). Although statistically significant differences were observed between the patent and control groups, it is important to note that the results in both groups were within established norms. The control group showed a larger range of variation, demonstrating the improved precision and consistency of our methodology.

7. SUMMARY

My PhD research culminated in a novel advancement in left ventricle assist device (LVAD) implantation. A highly effective 3D modelling environment was successfully constructed and assessed, facilitating the generation of patient-specific 3D models. This achievement has paved the way for innovative approaches to address challenges related to accurate inflow cannula insertion during durable LVAD implantation.

Our novel methodology focusing on the development and application of personalized 3D models, serving as crucial elements in preoperative decision-making and invaluable aids for precise surgical positioning tools, termed the "exoskeleton." Notably, our exoskeleton technology has obtained patent approvals in Hungary (91) and internationally (92), underscoring its uniqueness and innovation in the global scientific community.

To validate the clinical applicability and reproducibility of our findings, a comprehensive evaluation using engineering methodologies was conducted. Results revealed no statistically significant difference in volumetric accuracy between the virtual exoskeleton. Surface accuracy assessment, measuring maximum, median, and 95% Hausdorff values, demonstrated high precision, with maximum results ranging from 2.83mm ± 1.31mm and a 95th percentile consistently below 1mm.

Our results emphasize the remarkable congruence of the designed and 3D-printed exoskeletons, supporting their suitability as surgical equipment. In the clinical domain, an evaluation of alignment between intended implantation angles and postoperative results revealed a mean angle of 10.13° in the patent group, significantly different from the control group's mean of 22.87° ± 12.38° (p = 0.0208). Despite both cohorts falling within normal ranges, a subset of the control group exhibited higher variation, deviating from existing research parameters with a maximum deviation of 34.60°.

This discovery demonstrates enhanced consistency in durable LVAD implantation when employing the exoskeleton, in contrast to traditional device implantation. Further exploration is anticipated within a more extensive patient population to examine the clinical benefits associated with exoskeleton use on patient outcomes.

8. REFERENCES

1. Roger VL. Epidemiology of Heart Failure: A Contemporary Perspective. Circ Res. 2021;128(10):1421-34.

2. Tatum R, Briasoulis A, Tchantchaleishvili V, Massey HT. Evaluation of donor heart for transplantation. Heart Fail Rev. 2022;27(5):1819-27.

3. Fazekas L, Sax B, Hartyánszky I, Pólos M, Horkay F, Varga T, Rácz K, Németh E, Székely A, Paulovich E, Heltai K, Zima E, Szabolcs Z, Merkely B. [Mechanical circulatory support saves lives -- three years' experience of the newly established assist device program at Semmelweis University, Budapest, Hungary]. Orv Hetil. 2015;156(13):521-7.

4. Varshney AS, DeFilippis EM, Cowger JA, Netuka I, Pinney SP, Givertz MM. Trends and Outcomes of Left Ventricular Assist Device Therapy: JACC Focus Seminar. J Am Coll Cardiol. 2022;79(11):1092-107.

5. Dandel M, Hetzer R. Recovery of failing hearts by mechanical unloading: Pathophysiologic insights and clinical relevance. Am Heart J. 2018;206:30-50.

6. Englert JA, 3rd, Davis JA, Krim SR. Mechanical Circulatory Support for the Failing Heart: Continuous-Flow Left Ventricular Assist Devices. Ochsner J. 2016;16(3):263-9.

7. Sorensen EN, Kon ZN, Feller ED, Pham SM, Griffith BP. Quantitative Assessment of Inflow Malposition in Two Continuous-Flow Left Ventricular Assist Devices. Ann Thorac Surg. 2018;105(5):1377-83.

8. May-Newman K, Marquez-Maya N, Montes R, Salim S. The Effect of Inflow Cannula Angle on the Intraventricular Flow Field of the Left Ventricular Assist Device-Assisted Heart: An In Vitro Flow Visualization Study. Asaio j. 2019;65(2):139-47.

9. Chivukula VK, Beckman JA, Li S, Masri SC, Levy WC, Lin S, Cheng RK, Farris SD, Wood G, Dardas TF, Kirkpatrick JN, Koomalsingh K, Zimpfer D, Mackensen GB, Chassagne F, Mahr C, Aliseda A. Left Ventricular Assist Device Inflow Cannula Insertion Depth Influences Thrombosis Risk. Asaio j. 2020;66(7):766-73.

10. Pasrija C, Sawan MA, Sorensen E, Gammie JS, Madathil R, Tran D, Wang L, Ton VK, Feller E, Griffith BP, Kon ZN, Kaczorowski DJ. Inflow Cannula Position Influences

Improvement in Mitral Regurgitation After Ventricular Assist Device Implantation. Asaio j. 2021;67(4):423-9.

11.   Kortekaas KA, de Graaf MA, Palmen M, Braun J, Mertens BJA, Tops LF, Beeres SLMA. Left ventricular assist device and pump thrombosis: the importance of the inflow cannula position. Int J Cardiovasc Imaging. 2022;38(12):2771-9.

12.   Schlöglhofer T, Aigner P, Migas M, Beitzke D, Dimitrov K, Wittmann F, Riebandt J, Granegger M, Wiedemann D, Laufer G, Moscato F, Schima H, Zimpfer D. Inflow cannula position as risk factor for stroke in patients with HeartMate 3 left ventricular assist devices. Artif Organs. 2022;46(6):1149-57.

13.   Hariri IM, Dardas T, Kanwar M, Cogswell R, Gosev I, Molina E, Myers SL, Kirklin JK, Shah P, Pagani FD, Cowger JA. Long-term survival on LVAD support: Device complications and end-organ dysfunction limit long-term success. J Heart Lung Transplant. 2022;41(2):161-70.

14.   Mitrut R, Stepan AE, Pirici D. Histopathological Aspects of the Myocardium in Dilated Cardiomyopathy. Curr Health Sci J. 2018;44(3):243-9.

15.   Singh S, Takeda K, Kurlansky P. Left ventricular assist device positioning: a science that is far from exact. Eur J Cardiothorac Surg. 2022;62(4).

16.   Bertero E, Maack C. Metabolic remodelling in heart failure. Nat Rev Cardiol. 2018;15(8):457-70.

17.   Chan DZL, Kerr AJ, Doughty RN. Temporal trends in the burden of heart failure. Intern Med J. 2021;51(8):1212-8.

18.   Savarese G, Becher PM, Lund LH, Seferovic P, Rosano GMC, Coats AJS. Global burden of heart failure: a comprehensive and updated review of epidemiology. Cardiovasc Res. 2023;118(17):3272-87.

19.   Tomcsányi J, Toth L. National Health Insurance Fund Administration of Hungary. http://wwwoephu(Hungary). 2009.

20.   Nyolczas N, Heltai K, Borbély A, Habon T, Járai Z, Sziliczei E, Stadler P, Faludi R, Herczeg B, Papp E, Lakatos F, Nagy K, Katona A, Kovács I, Tomcsányi J, Nagy A, Sepp R. [Hungarian Heart Failure Registry 2015-2016. Preliminary results]. Orv Hetil. 2017;158(3):94-100.

21.   Bagyura Z, Kiss L, Edes E, Lux A, Polgár L, Soós P, Szenczi O, Szelid Z, Vadas R, Józan P, Bagdy G, Merkely B. [Cardiovascular screening programme in the Central Hungarian region. The Budakalász Study]. Orv Hetil. 2014;155(34):1344-52.

22.   Janaswamy P, Walters TE, Nazer B, Lee RJ. Current Treatment Strategies for Heart Failure: Role of Device Therapy and LV Reconstruction. Curr Treat Options Cardiovasc Med. 2016;18(9):57.

23.   Kuster GM, Pfister O. Chronic heart failure: advances in pharmacological treatment and future perspectives. Swiss Med Wkly. 2019;149:w20036.

24.   Hu LJ, Chen YQ, Deng SB, Du JL, She Q. Additional use of an aldosterone antagonist in patients with mild to moderate chronic heart failure: a systematic review and meta-analysis. Br J Clin Pharmacol. 2013;75(5):1202-12.

25.   Albert NM, Yancy CW, Liang L, Zhao X, Hernandez AF, Peterson ED, Cannon CP, Fonarow GC. Use of Aldosterone Antagonists in Heart Failure. JAMA. 2009;302(15):1658-65.

26.   Borek M, Charlap S, Frishman WH. Angiotensin-converting Enzyme Inhibitors in Heart Failure. Medical Clinics of North America. 1989;73(2):315-38.

27.   Shibata MC, Flather MD, Wang D. Systematic review of the impact of beta blockers on mortality and hospital admissions in heart failure. Eur J Heart Fail. 2001;3(3):351-7.

28.   Correale M, Monaco I, Tricarico L, Bottigliero D, Sicuranza M, Del Forno B, Godeas G, Teri A, Maiorano A, Perulli R, Centola A, De Bonis M, Di Biase M, Brunetti ND. Advanced heart failure: non-pharmacological approach. Heart Fail Rev. 2019;24(5):779-91.

29.   Ng GA, Mistry A, Newton M, Schlindwein FS, Barr C, Bates MG, Caldwell J, Das M, Farooq M, Herring N, Lambiase P, Osman F, Sohal M, Staniforth A, Tayebjee M, Tomlinson D, Whinnett Z, Yue A, Nicolson WB. Rationale and study design of the MINERVA study: Multicentre Investigation of Novel Electrocardiogram Risk markers in Ventricular Arrhythmia prediction-UK multicentre collaboration. BMJ Open. 2022;12(1):e059527.

30.   Lachlan T, He H, Sharma K, Khan J, Rajappan K, Morley-Davies A, Patwala A, Randeva H, Osman F. MAGNETO cardiography parameters to predict future Sudden

Cardiac Death (MAGNETO-SCD) or ventricular events from implantable cardioverter defibrillators: study protocol, design and rationale. BMJ Open. 2020;10(10):e038804.

31.   Atherton JJ. Chronic heart failure: we are fighting the battle, but are we winning the war? Scientifica (Cairo). 2012;2012:279731.

32.   Browne A, Gaines H, Alharethi R, Goodwin M, Selzman CH, Fang JC, Drakos SG, Stehlik J, Hanff TC. Interrupted Time Series Analysis of Donor Heart Use Before and After the 2018 UNOS Heart Allocation Policy Change. J Card Fail. 2023;29(2):220-4.

33.   de By TMMH, Mohacsi P, Gahl B, Zittermann A, Krabatsch T, Gustafsson F, Leprince P, Meyns B, Netuka I, Caliskan K, Castedo E, Musumeci F, Vincentelli A, Hetzer R, Gummert J; EUROMACS members. The European Registry for Patients with Mechanical Circulatory Support (EUROMACS) of the European Association for Cardio-Thoracic Surgery (EACTS): second report. Eur J Cardiothorac Surg. 2018;53(2):309-16.

34.   de By TMMH, Schoenrath F, Veen KM, Mohacsi P, Stein J, Alkhamees KMM, Anastasiadis K, Berhnardt A, Beyersdorf F, Caliskan K, Reineke D, Damman K, Fiane A, Gkouziouta A, Gollmann-Tepeköylü C, Gustafsson F, Hulman M, Iacovoni A, Loforte A, Merkely B, Musumeci F, Němec P, Netuka I, Özbaran M, Potapov E, Pya Y, Rábago G, Ramjankhan F, Reichenspurner H, Saeed D, Sandoval E, Stockman B, Vanderheyden M, Tops L, Wahlers T, Zembala M, Zimpfer D, Carrel T, Gummert J, Meyns B. The European Registry for Patients with Mechanical Circulatory Support of the European Association for Cardio-Thoracic Surgery: third report. Eur J Cardiothorac Surg. 2022;62(1).

35.   Chiumello D, Coppola S, Froio S, Colombo A, Del Sorbo L. Extracorporeal life support as bridge to lung transplantation: a systematic review. Critical Care. 2015;19(1):19.

36.   Hartyánszky I, Koppányi Á, Szabolcs Z, Horkay F, Fazekas L, Hüttl T, Pólos M, Daróczi L, Kőszegi A, Benke K, Tóth R, Kovács P, Barabás JI, Németh E, Édes IF, Merkely B. [The Semmelweis University extracorporeal membrane oxygenation program - 5 years' results and perspectives]. Orv Hetil. 2018;159(46):1876-81.

37.   Timms D. A review of clinical ventricular assist devices. Medical Engineering & Physics. 2011;33(9):1041-7.

38.   Krishnamani R, DeNofrio D, Konstam MA. Emerging ventricular assist devices for long-term cardiac support. Nature Reviews Cardiology. 2010;7(2):71-6.

39.   Conway J, Amdani S, Morales DLS, Lorts A, Rosenthal DN, Jacobs JP, Rossano J, Koehl D, Kirklin JK, Auerbach SR. Widening care gap in VAD therapy. J Heart Lung Transplant. 2023;42(12):1710-24.

40.   Lebreton G, Pozzi M, Mastroianni C, Léger P, Pavie A, Leprince P. Extracorporeal life support as a bridge to bridge: a strategy to optimize ventricular assist device results. European Journal of Cardio-Thoracic Surgery. 2015;48(5):785-91.

41.   Rousse N, Juthier F, Pinçon C, Hysi I, Banfi C, Robin E, Fayad G, Jegou B, Prat A, Vincentelli A. ECMO as a bridge to decision: Recovery, VAD, or heart transplantation? International Journal of Cardiology. 2015;187:620-7.

42.   Drakos SG, Kfoury AG, Stehlik J, Selzman CH, Reid BB, Terrovitis JV, Nanas JN, Li DY. Bridge to recovery: understanding the disconnect between clinical and biological outcomes. Circulation. 2012;126(2):230-41.

43.   Gyoten T, Rojas SV, Fox H, Schramm R, Hakim-Meibodi K, Ruiz-Cano M, Gummert JF, Morshuis M, Sandica E. Mechanical circulatory support as a bridge to candidacy in adults with transposition of the great arteries and a systemic right ventricle. Eur J Cardiothorac Surg. 2020;59(2):369-74.

44.   El-Banayosy A, Körfer R, Arusoglu L, Kizner L, Morshuis M, Milting H, Tenderich G, Fey O, Minami K. Device and patient management in a bridge-to-transplant setting. Ann Thorac Surg. 2001;71(3, Supplement 1):S98-S102.

45.   Komori M, Yamane T. Magnetic levitation system with a millimeter-sized cylindrical rotor. Mechatronics. 2000;10(6):595-607.

46.   Sidhu K, Lam PH, Mehra MR. Evolving trends in mechanical circulatory support: Clinical development of a fully magnetically levitated durable ventricular assist device. Trends Cardiovasc Med. 2020;30(4):223-9.

47.   Barabas Imre Janos MB, Hartyanszky Istvan, Palkovics Daniel Computer-aided Design and Manufacturing of a Patented, Left Ventricle Assist Device Positioning Tool – 3D Navigated Surgical Treatment of End-Stage Heart Failure. ACTA POLYTECHNICA HUNGARICA 2023;20(8):9-25.

48.   Molina EJ, Boyce SW. Current Status of Left Ventricular Assist Device Technology. Seminars in Thoracic and Cardiovascular Surgery. 2013;25(1):56-63.

49.   Pya Y, Abdiorazova A. Elimination of drive exit line: transcutaneous energy transmission. Ann Cardiothorac Surg. 2021;10(3):393-5.

50.   DeVore AD, Stewart GC. The Risk of Stroke on Left Ventricular Assist Device Support: Steady Gains or Stalled Progress? JACC Heart Fail. 2017;5(10):712-4.

51.   Aigner P, Schweiger M, Fraser K, Choi Y, Lemme F, Cesarovic N, Kertzscher U, Schima H, Hübler M, Granegger M. Ventricular Flow Field Visualization During Mechanical Circulatory Support in the Assisted Isolated Beating Heart. Ann Biomed Eng. 2020;48(2):794-804.

52.   Reider C, Moon J, Ramesh V, Montes R, Campos J, Herold B, Martinez-Legazpi P, Rossini L, del Alamo JC, Dembitsky W, May-Newman K. Intraventricular thrombus formation in the LVAD-assisted heart studied in a mock circulatory loop. Meccanica. 2017;52(3):515-28.

53.   Chivukula VK, Beckman JA, Prisco AR, Dardas T, Lin S, Smith JW, Mokadam NA, Aliseda A, Mahr C. Left Ventricular Assist Device Inflow Cannula Angle and Thrombosis Risk. Circ Heart Fail. 2018;11(4):e004325.

54.   Ghodrati M, Maurer A, Schlöglhofer T, Khienwad T, Zimpfer D, Beitzke D, Zonta F, Moscato F, Schima H, Aigner P. The influence of left ventricular assist device inflow cannula position on thrombosis risk. Artif Organs. 2020;44(9):939-46.

55.   Aziz W, Claridge S, Ntalas I, Gould J, de Vecchi A, Razeghi O, Toth D, Mountney P, Preston R, Rinaldi CA, Razavi R, Niederer S, Rajani R. Emerging role of cardiac computed tomography in heart failure. ESC Heart Fail. 2019;6(5):909-20.

56.   McDonagh TA, Metra M, Adamo M, Gardner RS, Baumbach A, Böhm M, Burri H, Butler J, Čelutkienė J, Chioncel O, Cleland JGF, Coats AJS, Crespo-Leiro MG, Farmakis D, Gilard M, Heymans S, Hoes AW, Jaarsma T, Jankowska EA, Lainscak M, Lam CSP, Lyon AR, McMurray JJV, Mebazaa A, Mindham R, Muneretto C, Francesco Piepoli M, Price S, Rosano GMC, Ruschitzka F, Kathrine Skibelund A; ESC Scientific Document Group. 2021 ESC Guidelines for the diagnosis and treatment of acute and chronic heart failure. Eur Heart J. 2021;42(36):3599-726.

57.   McDonagh TA, Metra M, Adamo M, Gardner RS, Baumbach A, Böhm M, Burri H, Butler J, Čelutkienė J, Chioncel O, Cleland JGF, Crespo-Leiro MG, Farmakis D, Gilard M, Heymans S, Hoes AW, Jaarsma T, Jankowska EA, Lainscak M, Lam CSP, Lyon AR, McMurray JJV, Mebazaa A, Mindham R, Muneretto C, Francesco Piepoli M, Price

S, Rosano GMC, Ruschitzka F, Skibelund AK; ESC Scientific Document Group. 2023 Focused Update of the 2021 ESC Guidelines for the diagnosis and treatment of acute and chronic heart failure. Eur Heart J. 2023;44(37):3627-39.

58.   Acharya D, Aryal S, Loyaga-Rendon R, Pamboukian SV, Tallaj J, Kirklin JK, Holman WL, Singh S. Use of Computed Tomography in Preoperative Planning for Heartware Left Ventricular Assist Device Placement. Asaio j. 2019;65(1):70-6.

59.   Farooqi KM, Saeed O, Zaidi A, Sanz J, Nielsen JC, Hsu DT, Jorde UP. 3D Printing to Guide Ventricular Assist Device Placement in Adults With Congenital Heart Disease and Heart Failure. JACC Heart Fail. 2016;4(4):301-11.

60.   Raman SV, Sahu A, Merchant AZ, Louis LBt, Firstenberg MS, Sun B. Noninvasive assessment of left ventricular assist devices with cardiovascular computed tomography and impact on management. J Heart Lung Transplant. 2010;29(1):79-85.

61.   Li X, Kondray V, Tavri S, Ruhparwar A, Azeze S, Dey A, Partovi S, Rengier F. Role of imaging in diagnosis and management of left ventricular assist device complications. Int J Cardiovasc Imaging. 2019;35(7):1365-77.

62.   He K, Gan C, Li Z, Rekik I, Yin Z, Ji W, Gao Y, Wang Q, Zhang J, Shen D. Transformers in medical image analysis. Intelligent Medicine. 2023;3(1):59-78.

63.   Bui I, Bhattacharya A, Wong SH, Singh HR, Agarwal A. Role of Three-Dimensional Visualization Modalities in Medical Education. Front Pediatr. 2021;9:760363.

64.   Han H, Han X, Gao T. 3D mesh model segmentation based on skeleton extraction. The Imaging Science Journal. 2021;69(1-4):153-63.

65.   Beitler BG, Abraham PF, Glennon AR, Tommasini SM, Lattanza LL, Morris JM, Wiznia DH. Interpretation of regulatory factors for 3D printing at hospitals and medical centers, or at the point of care. 3D Print Med. 2022;8(1):7.

66.   Barabás JI, Ghimessy ÁK, Rényi-Vámos F, Kocsis Á, Agócs L, Mészáros L, Pukacsik D, Andi J, Laki A, Vörös F, Hartyánszky I, Panajotu A, Fazekas L, Szabolcs Z, Merkely B. [Innovation in medicine: opportunities of 3D modeling and printing for perioperative care of cardio and thoracic surgical patients. Experiences in Hungary]. Orv Hetil. 2019;160(50):1967-75.

67.   Blanco I. The Use of Composite Materials in 3D Printing. Journal of Composites Science. 2020;4(2):42.

68.	Layani M, Wang X, Magdassi S. Novel Materials for 3D Printing by Photopolymerization. Adv Mater. 2018;30(41):e1706344.

69.	Das S, Bourell DL, Babu SS. Metallic materials for 3D printing. MRS Bulletin. 2016;41(10):729-41.

70.	Arefin AME, Khatri NR, Kulkarni N, Egan PF. Polymer 3D Printing Review: Materials, Process, and Design Strategies for Medical Applications. Polymers. 2021;13(9):1499.

71.	Chivukula VK, Beckman JA, Prisco AR, Lin S, Dardas TF, Cheng RK, Farris SD, Smith JW, Mokadam NA, Mahr C, Aliseda A. Small Left Ventricular Size Is an Independent Risk Factor for Ventricular Assist Device Thrombosis. Asaio j. 2019;65(2):152-9.

72.	Cheung JP, Shugard E, Mistry N, Pouliot J, Chen J. Evaluating the impact of extended field-of-view CT reconstructions on CT values and dosimetric accuracy for radiation therapy. Med Phys. 2019;46(2):892-901.

73.	Maolood IY, Al-Salhi YEA, Lu S. Thresholding for Medical Image Segmentation for Cancer using Fuzzy Entropy with Level Set Algorithm. Open Med (Wars). 2018;13:374-83.

74.	Goliaei S, Ghorshi S, Manzuri MT, Mortazavi M, editors. A Kalman filter technique applied for medical image reconstruction. Eighth International Multi-Conference on Systems, Signals & Devices; 2011 22-25 March 2011.

75.	Vyavahare S, Teraiya S, Panghal D, Kumar S. Fused deposition modelling: a review. Rapid Prototyping Journal. 2020;26(1):176-201.

76.	Huang J, Qin Q, Wang J. A Review of Stereolithography: Processes and Systems. Processes. 2020;8(9):1138.

77.	Mazzoli A. Selective laser sintering in biomedical engineering. Medical & Biological Engineering & Computing. 2013;51(3):245-56.

78.	Krithika Alias AnbuDevi M, Suganthi K. Review of Semantic Segmentation of Medical Images Using Modified Architectures of UNET. Diagnostics (Basel). 2022;12(12).

79.	Taha AA, Hanbury A. Metrics for evaluating 3D medical image segmentation: analysis, selection, and tool. BMC Med Imaging. 2015;15:29.

80.   World Medical Association Declaration of Helsinki: ethical principles for medical research involving human subjects. Jama. 2013;310(20):2191-4.

81.   Barabás IJ, Hartyánszky I, Kocher A, Merkely B. A 3D printed exoskeleton facilitates HeartMate III inflow cannula position. Interact Cardiovasc Thorac Surg. 2019;29(4):644-6.

82.   Barabás JI, Palkovics D, Bognár V, Sax B, Heltai K, Panajotu A, Merkely B, Hartyánszky I. [The role of 3D technology in the support of mechanical circulation therapy.]. Orv Hetil. 2023;164(26):1026-33.

83.   Hartyánszky I, Tóth A, Berta B, Pólos M, Veres G, Merkely B, Szabolcs Z, Pepper J. Personalized surgical repair of left ventricular aneurysm with computer-assisted ventricular engineering. Interact Cardiovasc Thorac Surg. 2014;19(5):801-6; discussion 806.

84.   Benke K, Barabás JI, Daróczi L, Sayour AA, Szilveszter B, Pólos M, Lux Á, Székely A, Radovits T, Hartyánszky I, Merkely B, Szabolcs Z. Routine aortic valve replacement followed by a myriad of complications: role of 3D printing in a difficult cardiac surgical case. J Thorac Dis. 2017;9(11):E1021-e4.

85.   Shi L, Sun J, Yang Y, Ling T, Wang M, Gu Y, Yang Z, Hua Y, Zhang J. Three-Dimensional Visual Patient Based on Electronic Medical Diagnostic Records. IEEE J Biomed Health Inform. 2018;22(1):161-72.

86.   Langridge B, Momin S, Coumbe B, Woin E, Griffin M, Butler P. Systematic Review of the Use of 3-Dimensional Printing in Surgical Teaching and Assessment. J Surg Educ. 2018;75(1):209-21.

87.   Yang M, Li C, Li Y, Zhao Y, Wei X, Zhang G, Fan J, Ni H, Chen Z, Bai Y, Li M. Application of 3D rapid prototyping technology in posterior corrective surgery for Lenke 1 adolescent idiopathic scoliosis patients. Medicine (Baltimore). 2015;94(8):e582.

88.   Liu YF, Xu LW, Zhu HY, Liu SS. Technical procedures for template-guided surgery for mandibular reconstruction based on digital design and manufacturing. Biomed Eng Online. 2014;13:63.

89.   Crumpstone T, Martin TD, Yang JJ, Peng YG. Misplacement of LVAD inflow cannula leads to insufficient output and tissue hypoperfusion. J Artif Organs. 2010;13(4):225-7.

90.   Cowger JA, Stulak JM, Shah P, Dardas TF, Pagani FD, Dunlay SM, Maltais S, Aaronson KD, Singh R, Mokadam NA, Kirklin JK, Salerno CT. Impact of Center Left Ventricular Assist Device Volume on Outcomes After Implantation: An INTERMACS Analysis. JACC Heart Fail. 2017;5(10):691-9.

91.   Hartyánszky István, Barabás János Imre, Merkely Béla. Körkés pozicionálását elősegítő héj, eljárás a héj előállítására, eljárás a héj alkalmazására műtéti eljárás szimulációja során

Benyújtás éve (szabadalom): 2018, Benyújtás száma: A61M 1/12, Ügyszám: P 18 00379, Benyújtás országa: Magyarország, Magyar szabadalom (Oltalmi formák). 2018.

92.   Hartyánszky István, Barabás János Imre, Merkely Béla. Pozícionálást elősegítő szerkezet, eljárás a szerkezet előállítására, eljárás a szerkezet alkalmazására műtéti eljárás és/vagy annak szimulációja során

P1800379, Benyújtás éve (szabadalom): 2018, Benyújtás száma: 311174000-20181109-1249-013198, Ügyszám: A61M 1/12, Benyújtás országa: Magyarország Magyar szabadalom (Oltalmi formák). 2018.

93.   May-Newman K, Montes R, Campos J, Marquez-Maya N, Vu V, Zebrowski E, Motomura T, Benkowski R. Reducing regional flow stasis and improving intraventricular hemodynamics with a tipless inflow cannula design: An in vitro flow visualization study using the EVAHEART LVAD. Artif Organs. 2019;43(9):834-48.

9. BIBLIOGRAPHY

9.1. Publications discussed in the present thesis

Barabas Imre Janos, Merkely Bela, Hartyanszky Istvan, Palkovics Daniel
Computer-aided Design and Manufacturing of a Patented, Left Ventricle Assist Device
Positioning Tool – 3D Navigated Surgical Treatment of End-Stage Heart Failure
ACTA POLYTECHNICA HUNGARICA 20: 8 pp. 9-25. (2023), IF: **1,7***
*Expected IF value

Barabás János Imre, Palkovics, Dániel, Bognár Viktória, Sax Balázs, Heltai Krisztina,
Panajotu Alexisz, Merkely Béla, Hartyánszky István
A 3D technológia szerepe a műszívterápiában: Semmelweis Szabadalom [The role of 3D
technology in the support of mechanical circulation therapy Semmelweis Patent]
ORVOSI HETILAP 164: 26 pp. 1026-1033. (2023), IF: 0,6*
*Expected IF value

Barabás Imre János, Hartyánszky István, Kocher Alfred, Merkely Béla
A 3D printed Exoskeleton facilitates HeartMate III inflow cannula position
INTERACTIVE CARDIOVASCULAR AND THORACIC SURGERY 29: 4 pp.
644-646. (2019), **IF: 1,675**

Barabás János Imre, Ghimessy Áron Kristóf, Rényi-Vámos Ferenc, Kocsis Ákos,
Agócs László, Mészáros László, Pukacsik Dávid, Andi Judit, Laki András, Vörös Fanni,
Hartyánszky István, Panajotu Alexis, Fazekas Levente, Szabolcs Zoltán, Merkely Béla
Innovációs lehetőségek a medicinában: 3D tervezési és 3D nyomtatási lehetőségek a
felnőtt szív- és mellkassebészeti betegellátásban: Magyarországi tapasztalatok
[Innovation in medicine opportunities of 3D modeling and printing for perioperative care
of cardio and thoracic surgical patients. Experiences in Hungary]
ORVOSI HETILAP 160: 50 pp. 1967-1975. (2019), **IF: 0,4971**

Hartyánszky István, **Barabás János Imre**, Merkely Béla

Körkés pozicionálását elősegítő héj, eljárás a héj előállítására, eljárás a héj alkalmazására műtéti eljárás szimulációja során

Benyújtás éve (**szabadalom**): 2018, Benyújtás száma: A61M 1/12, Ügyszám: P 18 00379, Benyújtás országa: Magyarország, Magyar szabadalom (Oltalmi formák)

Hartyánszky István, **Barabás, János Imre**, Merkely Béla

Pozícionálást elősegítő szerkezet, eljárás a szerkezet előállítására, eljárás a szerkezet alkalmazására műtéti eljárás és/vagy annak szimulációja során

P1800379, Benyújtás éve (**szabadalom**): 2018, Benyújtás száma: 311174000-20181109-1249-013198, Ügyszám: A61M 1/12, Benyújtás országa: Magyarország Magyar szabadalom (Oltalmi formák)

Barabás János Imre, Pólos Miklós, Daróczi László, Hüttl Tivadar, Benke Kálmán, Horkay Ferenc, Szabolcs Zoltán, Hartyánszky István

Számítástechnikai döntéstámogató rendszer kiépítése a szívsebészetben: a 3D tervezéstől a posztoperatív eredményekig [Computer-assisted decision-making in cardiac surgery: from 3D preoperative planning to computational fluid dynamics in the design of surgical procedures]

MAGYAR SEBÉSZET 71: 3 pp. 117-125. (2018)

9.2. Publications not related to the present thesis

Benke Kálmán*, Barabás János Imre*, Daróczi László, Sayour Ali, Szilveszter Bálint, Pólos Miklós, Lux Árpád, Székely Andrea, Radovits Tamás, Hartyánszky István, Merkely Béla, Szabolcs, Zoltán

Routine aortic valve replacement followed by a myriad of complications: role of 3D printing in a difficult cardiac surgical case

JOURNAL OF THORACIC DISEASE 9: 11 pp. E1021-E1024. (2017), **IF: 1,804**

*First authors shared

Hartyánszky István, Sax Balázs, Fazekas Levente, Szabolcs Zoltán, Horkay Ferenc, Heltai Krisztina, Németh Endre, Hüttl Tivadar, Pólos Miklós, Daróczi László, Kőszegi Andrea, Tóth Roland, **Barabás János Imre**, Benke Kálmán, Kovács Péter, Merkely Béla

A mechanikus keringéstámogatás helyzete Magyarországon a Városmajor eredményeinek tükrében

CARDIOLOGIA HUNGARICA 47: 2 pp. 112-118. (2017)

Szentmihályi Ilona, **Barabás János Imre**, Bali Ágnes, Kapus Gábor, Tamás Csilla, Sax Balázs, Németh Endre, Pólos Miklós, Daróczi László, Kőszegi Andrea, Cao Chun, Benke Kálmán, Kovács Péter, Fazekas Levente, Szabolcs Zoltán, Merkely Béla, Hartyánszky István

Szívtranszplantáció és műszívkezelés költséghatékonysági elemzési modellje: [Heart transplantation and long-term lvad support cost-effectiveness model]

MAGYAR SEBÉSZET 69: 4 pp. 186-193. (2016)

Barabás János Imre, Hüttl Tivadar, Hartyánszky István, Fazekas Levente, Oláh Zoltán, Zima Endre, Paulovich Erzsébet, Kőszegi Andrea, Szabolcs Zoltán

Hasüregbe vándorolt epicardialis pacemaker [Migration of an epicardial pacemaker into the abdominal cavity. Case report]

ORVOSI HETILAP 156: 4 pp. 154-157. (2015), **IF: 0,291**

10. ACKNOWLEDGEMENT